REPORT DOCUMENTATION PAGE

1a. REPORT SECURITY CLASSIFICATION UNCLASSIFIED	1b. RESTRICTIVE MARKINGS
2a. SECURITY CLASSIFICATION AUTHORITY	3. DISTRIBUTION/AVAILABILITY OF REPORT APPROVED FOR PUBLIC RELEASE;DISTRIBUTION UNLIMITED.
2b. DECLASSIFICATION/DOWNGRADING SCHEDULE	
4. PERFORMING ORGANIZATION REPORT NUMBER(S)	5. MONITORING ORGANIZATION REPORT NUMBER(S)
6a. NAME OF PERFORMING ORGANIZATION NAVAL POSTGRADUATE SCHOOL 6b. OFFICE SYMBOL (*If applicable*) ME	7a. NAME OF MONITORING ORGANIZATION NAVAL POSTGRADUATE SCHOOL
6c. ADDRESS (*City, State, and ZIP Code*) MONTEREY,CA 93943-5000	7b. ADDRESS (*City, State, and ZIP Code*) MONTEREY,CA 93943-5000
8a. NAME OF FUNDING/SPONSORING ORGANIZATION 8b. OFFICE SYMBOL (*If applicable*)	9. PROCUREMENT INSTRUMENT IDENTIFICATION NUMBER
8c. ADDRESS (*City, State, and ZIP Code*)	10. SOURCE OF FUNDING NUMBERS Program Element No / Project No / Task No / Work Unit Accession Number

11. TITLE (*Include Security Classification*)
Determination of GTA Welding Efficiencies

12. PERSONAL AUTHOR(S) Franche, Candonino P.

13a. TYPE OF REPORT	13b. TIME COVERED	14. DATE OF REPORT (*year, month, day*)	15. PAGE COUNT
Master's Thesis in M.E.	From : March 1992 To: March 1993	1993March25	74

16. SUPPLEMENTARY NOTATION
The views expressed in this thesis are those of the author and do not reflect the official policy or position of the Department of Defense or the U.S. Government.

17. COSATI CODES			18. SUBJECT TERMS (*continue on reverse if necessary and identify by block number*)
FIELD	GROUP	SUBGROUP	Laser Arc Welding, Solidification Parameters, Numerical Methods, Determining Welding Efficiencies.

19. ABSTRACT (*continue on reverse if necessary and identify by block number*)

A method is developed for estimating welding efficiencies for moving arc GTAW processes. Under quasi-conditions, the net heat transfer rate from the weld pool to the workpiece is estimated from a 3-D numerical heat transfer conduction model. The dimensions of the weld pool used in the computational model are obtained experimentally using a laser vision system and by metallurgical examination. The welding efficiency is then calculated by dividing the net heat transfer rate by the total power input during the experiments. Efficiencies are measured for a range of power inputs and torch speeds and then compared with those available in the literature.

20. DISTRIBUTION/AVAILABILITY OF ABSTRACT	21. ABSTRACT SECURITY CLASSIFICATION	
☒ UNCLASSIFIED/UNLIMITED ☐ SAME AS REPORT ☐ DTIC USERS	Unclassified	
22a. NAME OF RESPONSIBLE INDIVIDUAL Professor Yogendra Joshi	22b. TELEPHONE (*Include Area code*) 408-656-3400	22c. OFFICE SYMBOL ME/Ji

DD FORM 1473, 84 MAR — 83 APR edition may be used until exhausted. All other editions are obsolete.

Approved for public release; distribution is unlimited.

Determination of GTA
Welding Efficiencies

by

Candonino P. Franche
Lieutenant, United States Navy
B.S.M.E. FEATI University, Philippines, 1974
M.B.A., National University, San Diego, CA., 1990

Submitted in partial fulfillment
of the requirements for the degree of

MASTER OF SCIENCE IN MECHANICAL ENGINEERING

from the

NAVAL POSTGRADUATE SCHOOL
March 1993

ABSTRACT

A method is developed for estimating welding efficiencies for moving arc GTAW processes. Under quasi-steady conditions, the net heat transfer rate from the weld pool to the workpiece is estimated from a 3-D numerical heat transfer conduction model. The dimensions of the weld pool used in the computational model are obtained experimentally using a laser vision system and by metallurgical examination. The welding efficiency is then calculated by dividing the net heat transfer rate by the total power input during the experiments. Efficiencies are measured for a range of power inputs and torch speeds and then compared with those available in the literature.

TABLE OF CONTENTS

LIST OF FIGURES

LIST OF TABLES

ACKNOWLEDGEMENTS

The author wishes to extend his sincere appreciation to those who personally helped him throughout the research and development of his thesis at the Naval Postgraduate School.

A special thanks is expressed to the following: Mardo Blanco for helping and assisting in cutting the steels; Thomas McCord and the staff of the Mechanical Engineering Machine Shop for their unselfish time to ensure that the machine shop was ready for my use; and to Doug Shelton for providing materials for polishing, etching and taking optical microscopy of the weld metals.

A sincere thanks is also given to the Curricular Officer Captain Ericson for making me earn my Master's Degree and to Pam for her helpful administrative matters.

My heartfelt gratitude is given to Professor Yogendra Joshi and most especially to Dr. Pradip Dutta on their constant and personal advice, without them the development of my thesis will be impossible.

Finally, most credit for my accomplishment is passed on to my wife Gemma and my wonderful children Marissa, Don Joseph and Jonathan who gave all the support throughout the duration of my studies while leaving them behind in San Diego.

I. INTRODUCTION

A. THE NEED FOR WELDING EFFICIENCY

Since the inception of gas tungsten arc welding (GTAW) process was first patented in 1890 by C.L. Coffin [Ref. 1], there have been significant advances both in theoretical and experimental research in understanding the numerous factors affecting arc welding operations. Heat flow in the workpiece during arc welding strongly affects not only the weld pool geometry but also the microstructure and mechanical properties of the resultant weld.

As shown in Figure 1, a fraction of the power dissipation in the arc is lost to the surroundings and the remaining thermal energy input to the workpiece causes the formation of the weld pool. Indeed, knowing the fraction of power dissipated that is actually absorbed by the workpiece is essential in any predictions of weld pool geometry and resulting metallurgical properties. The present study is directed towards the development of a systematic method for the determination of the fraction of the net power transferred to the workpiece as the welding efficiency. A combined experimental and numerical approach is proposed. The proposed numerical model along with the data gathered from the experiments allow the calculation of welding arc efficiencies.

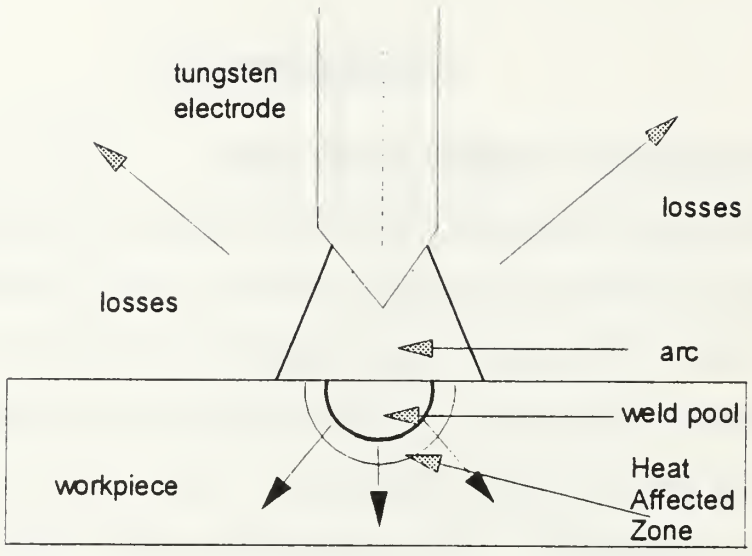

Figure 1. Energy Distribution of the Welding Arc.

B. PREVIOUS DETERMINATIONS OF WELDING EFFICIENCY

The existing estimates of welding efficiencies are based either on analytical/numerical methods or calorimetric measurements. The former are based on the pioneering work of Rosenthal. Rosenthal [Ref. 2] obtained the analytical solution for several idealized welding heat sources. These included moving point, line and plane heat sources within solid media. His studies were based on the constant properties heat conduction equation which transformed to the Stelmholtz equation under quasi-steady state conditions. The welding efficiency can be calculated as the ratio of the heat

transfer rate to the workpiece and the power dissipation from the source:

$$\eta = Q/EI$$

where: Q = heat rate transferred to the workpiece

E = Voltage across arc welding

I = Current

Q can be estimated by using Rosenthal's [Refs. 3-4] solution for two dimensional heat distributions for relatively thin plates as follows:

$$Q=[\exp(\frac{Ux}{2\alpha_s})K_0(\frac{UR}{2\alpha_s})]/2\pi(T-T_0)K_sG$$

For thick plates, three-dimensional heat distribution in an infinitely thick plate yields:

$$Q=\frac{\exp[\frac{-U(R-x)}{2\alpha_s}]}{2\pi(T-T_0)K_sR}$$

where:

T = Temperature of the point in question

T_0 = Initial Temperature at the point in question

K_s = Thermal conductivity of the workpiece and assumed constant

G = Thickness of the workpiece

U = Rate of travel of the arc

α_s= Thermal diffusivity of the workpiece and

assumed to be constant

K_0= Modified Bessel Function of the second kind and zero order, and

R = Distance from the point in question to the heat source.

The above equations have been used extensively by researchers but the methodology has drawbacks because Rosenthal's solutions assume (1) idealized heat sources, (2) no melting and negligible heat of fusion, (3) constant thermal properties, and (4) no heat loss from the workpiece surfaces [Ref. 5]. Cristensen et al.[Ref. 6] used the Rosenthal's point source solution and computed welding efficiencies using the weld pool geometry and welding conditions. For the GTA welding process a wide range from 21 to 48% was found. Ushio et al.[Ref. 7] also had used the Rosenthal point source solution and found similar results. Grosh and Travant, [Ref. 8] investigated experimentally and analytically the quasi-stationary temperature distributions within a thin and thick plates. Pavelic et al.[Ref. 9] introduced a finite area distributed heat source into the welding analysis and carried out a finite difference solution of the governing equations. They used a radially symmetric Gaussian distribution as the heat input from the welding arc. Tsai [Refs. 10-11] extended the solution by Grosh by using finite heat sources.

A recent effort by Wilkinson and Milner [Ref. 12] estimates the heat transfer rate from an arc to a workpiece

during GTA welding using the cathode-anode theory. They assumed the electrode to be the cathode and the workpiece (water cooled) to be the anode. The number of electrons were postulated to be proportional to the rate of heat transfer to the anode. Welding efficiencies were computed based on gathered measurements of heat transfer to the anode for an arc of zero length. Increasing the arc length decreased overall efficiency of the arc due to convection and radiation. They reported efficiencies with this type of technique from 80 to 90%. Malmuth et al. [Ref. 13] and Tsai and Eager [Ref. 14] used the same technique and reported values ranging from 83 to 90% by varying the current input.

Other calorimetric measurements have also been reported by Giedt et al [Ref. 15]. The energy transfer to the workpiece is determined by immersing the workpiece in liquid nitrogen immediately after a weld is completed. The amount of liquid vaporized gives the total thermal energy transferred to the workpiece. Giedt et al. [Ref. 15] measured a mean welding arc efficiency of 80%. Smartt et al. [Ref. 16] using the same equipment measured welding arc efficiencies that ranged from 71-84%.

C. PRESENT METHOD FOR OBTAINING WELDING EFFICIENCY

The technique developed in the present thesis uses a combined experimental and computational approach for the determination of the welding efficiency. The shape and size

of the weld pool is determined experimentally during quasi-steady conditions using free surface visualization and post solidification metallurgical examination. The weld pool geometry is then approximated by a double ellipsoidal shape. This shape, seen in Figure 2, has been used by Goldak et al [Ref. 17] for computations of welding thermal histories.

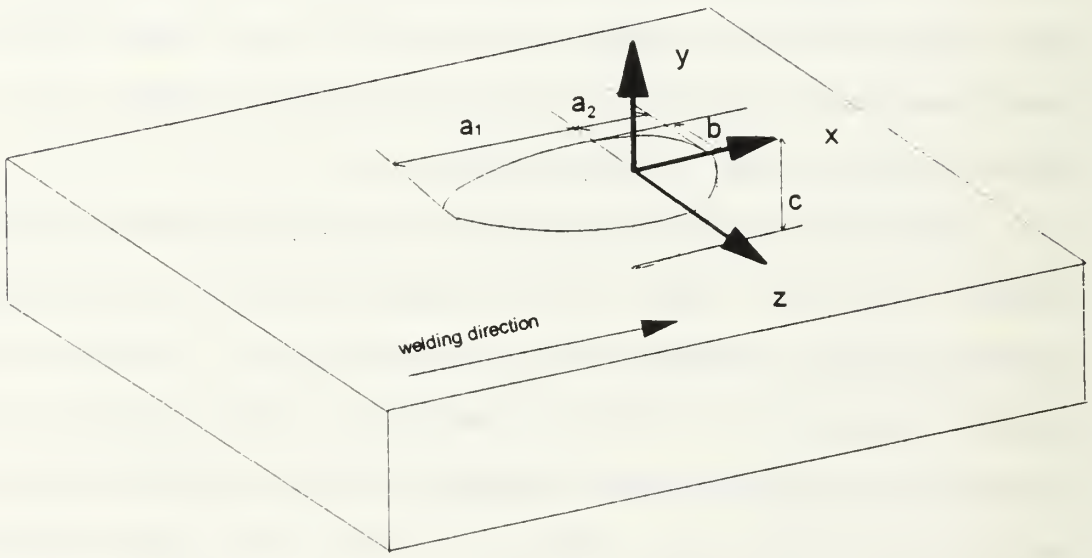

Figure 2. Double Ellipsoid Heat Source Configuration.

Using a three-dimensional, computational finite difference model, the temperature field within the workpiece, outside the weld pool is determined. The use of this approach allows the relaxation of a number of idealizations made in other

estimation of the welding efficiency. The efficiency is computed by finding the net heat transfer rate into the parent material from the weld pool boundary. In the following, the experimental and the numerical techniques employed are described in detail.

II. EXPERIMENTAL APPARATUS, MATERIALS, AND PROCEDURES

A. GAS TUNGSTEN ARC WELDING APPARATUS

Gas tungsten arc welding (GTAW) is an arc welding process that produces coalescence of metals by heating them with an arc between a nonconsumable tungsten electrode and the workpiece. Figure 3 is a sketch of the Direct Current Straight Polarity (DCSP)GTAW process with all its associated components as used in the present study. In this arrangement the electrons emitted from the tungsten electrode are accelerated to a very high speed while traveling through the arc. These high speed electrons bombard the workpiece and provide large surface heat fluxes resulting in a well defined molten region called the weld pool. A 2% thoriated tungsten electrode was used in the experiments because it has a higher electron emissivity and better current carrying capacity than pure tungsten electrodes [Ref. 18]. Argon gas flow rates of 196 -220 milliliters per second (25 to 28 cubic feet per hour) were used during the process.

B. WELD METAL PROPERTIES

With a carbon content of 0.12 - 0.18 %, the HY-80 steel is considered a mild steel. Typical chemical composition of the HY-80 is shown in Table I. This steel was chosen for the present experiments because it is widely used in the

GAS TUNGSTEN ARC WELDING PROCESS (SCHEMATIC)

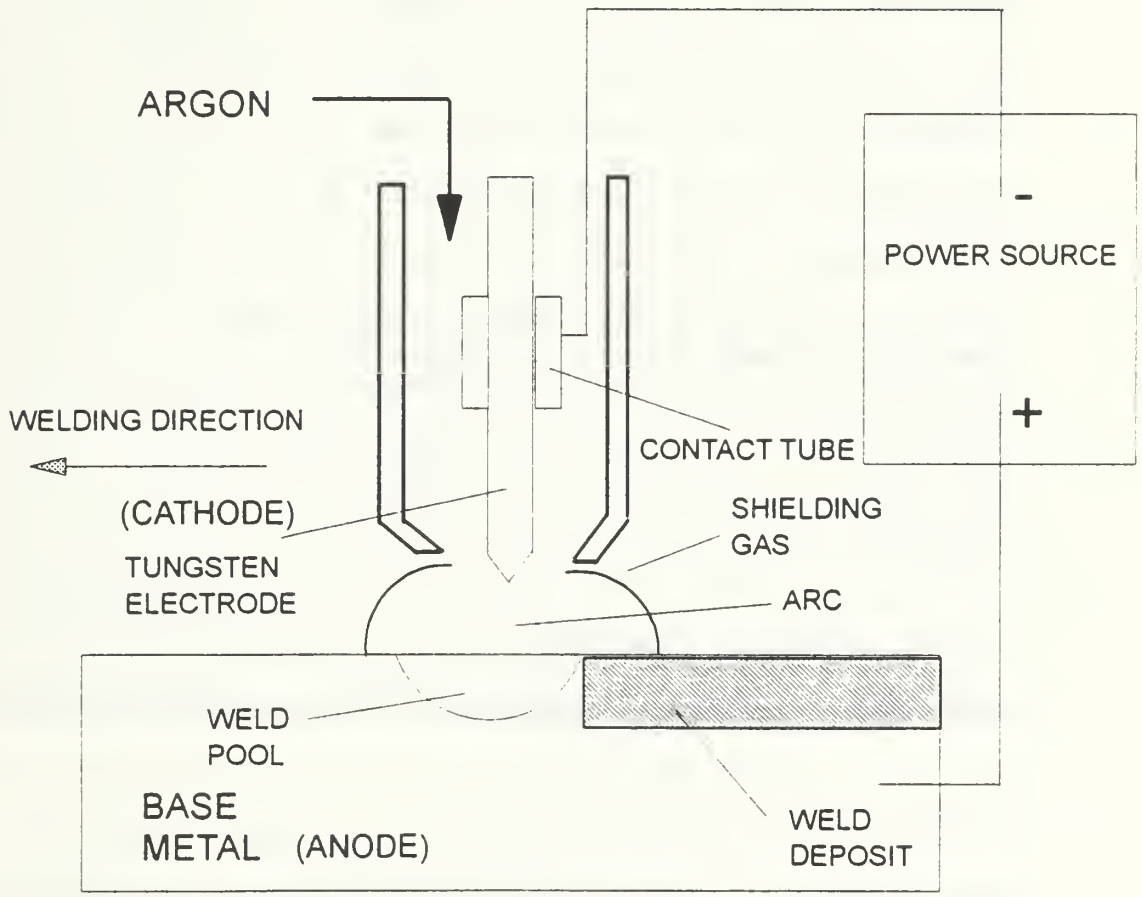

Figure 3. Sketch of the Gas Tungsten Arc Welding Process.

Table I. CHEMICAL COMPOSITION OF HY-80 STEEL.

ELEMENT	PERCENT
Carbon	0.12 - 0.18
Manganese	0.10 - 0.40
Phosphorus	0.025
Sulfur	0.025
Silicon	0.15 - 0.35
Nickel	2.00 - 3.25
Chromium	1.00 - 1.80
Molybdenum	0.20 - 0.60

Residual Elements	Percent
Titanium	0.02
Vanadium	0.03
Copper	0.25

construction of naval vessels and ordnance equipment. This type of steel is intended for service conditions that comprise dynamic loading. When welded properly, HY-80 joint strength and toughness approach that of the base metal and the joints are durable enough to withstand ballistic loading any

failure. This steel is manufactured with specification of MIL-S-16216 (Ships).

C. WELD POOL VISUALIZATION

The arc during the welding process was so bright that intense external illumination with spectral filtering must be used to view and record the weld pool free surface. The purpose of the Model PN-232 Laser Augmented Welding Vision System (Control Vision, Inc.) is to overcome the undue variation in scene brightness created by the welding arc. The pulsed ultra violet laser signal reflected from the workpiece is much brighter than the direct and reflected light of the welding arc. The system uses a special purpose video camera equipped with a CCD video sensor and a very high speed electronic shutter. The shutter is synchronized with the laser flash. Each laser flash is triggered once per video frame and lasts for a duration of approximately 3 *n*s. The system is also equipped with a narrow-band optical filter to match the laser wavelength which further suppresses the arc lighting. The net combination of both the temporal and spectral filtering results in a video image that is almost free of the unfavorable arc lighting effects. The complete system consists of a pulsed nitrogen laser unit, a camera unit, a solid state television, and a system controller that are interconnected by various electrical and fiberoptic cables [Ref. 19] as shown in Figure 4.

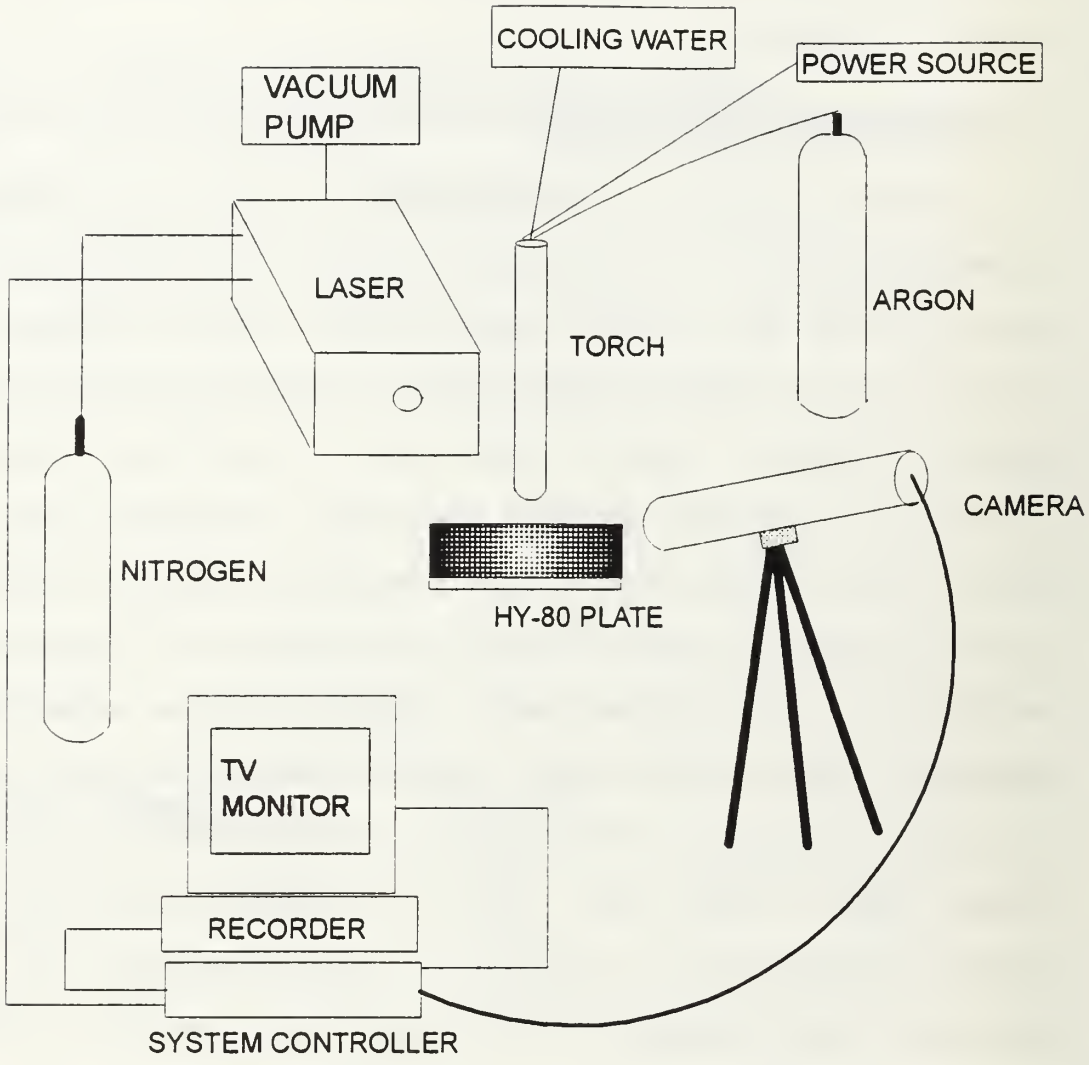

Figure 4. Laser Augmented Welding Vision System.

1. Laser Unit

The pulsed nitrogen laser is a PRA/Model UV12 manufactured by PRA Laser Inc., Ontario, Canada. The optical laser radiation has an operating wavelength of 337 nm (near-visible ultraviolet region in the spectrum) with 3 *ns* duration pulses, 60 Hz and a power level of 90 mW. For operation, the

laser requires an external vacuum pump that is capable of maintaining 60 torr [Ref. 20]. A nitrogen supply to the laser is continuously maintained at 275 - 315 milliliter/second (35-40 cubic feet/hour). Figure 5 and 6 are the photographs of the laser and the vacuum pump respectively.

Figure 5. Laser Photonics PRA/Model UV12 Pulsed Nitrogen Laser.

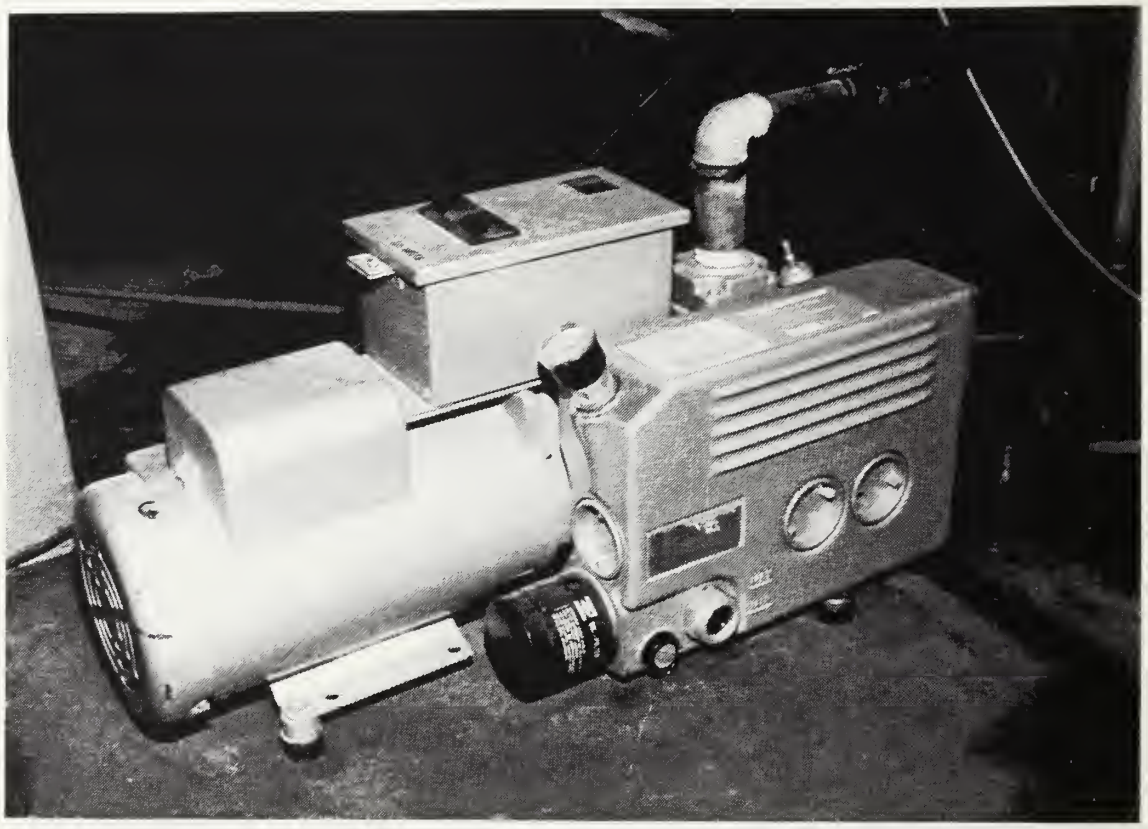

Figure 6. Vacuum Pump, Manufactured by Bosch, Inc.

2. Camera Unit

The camera contains a standard end-viewing optical head which interfaces directly with the image intensifier tube that is integrated within the camera. The camera optics is protected from smoke and spatter by use of a fused quartz window installed at the front face of the optical head. Also, inside the camera are the objective lens elements, spectral bandpass filter, and an iris diaphragm. The camera unit is shown in Figure 7. The camera is located about 6 to 8 inches from the weld site for the best field-of-view (FOV).

Figure 7. Camera Unit.

The FOV can be adjusted by appropriate refocusing of the lens barrel. Figure 8 shows the camera set up with the torch and the workpiece. The camera unit is controlled by the system controller to which it is connected via fiber optic cable.

3. System Controller

The system controller is manufactured by Control Vision System, Idaho Falls, Idaho. It can be regulated to send the appropriate trigger commands to pulse the laser and initiate shuttering of the camera unit. Electronic delay

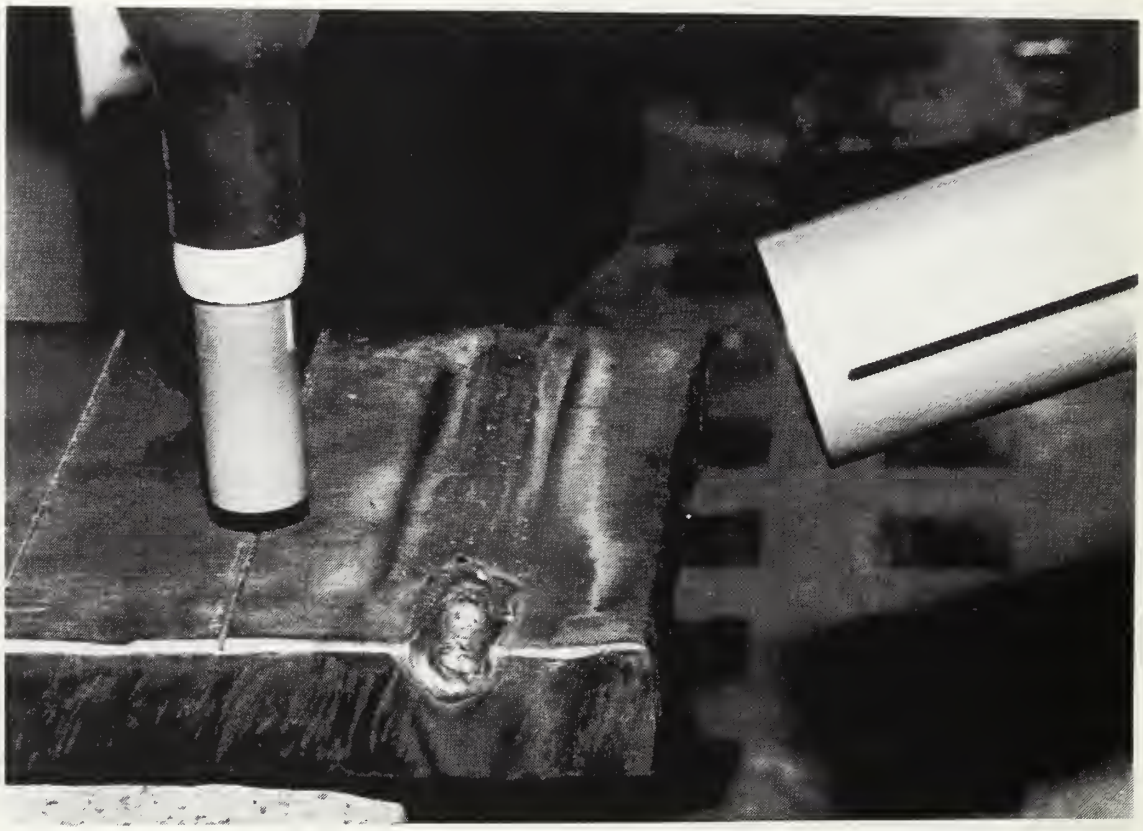

Figure 8. Camera Unit, Torch, and Weldpiece Set-up.

between the laser and the shutter unit required the setting of the shutter delay of .38 μs. The controller provides power to the camera unit and serve for manual adjustments of the shutter speed, video frame rate, and sensitivity.

4. TV Monitor and Video Recorder

The TV monitor model TR-196M was a Panasonic black and white with a 19-inch screen. Frame by frame playback was done by a VHS Panasonic Time Lapse Recorder Model AG-6720-P which was used for the determination of weld pool sizes. Output

Figure 9. TV Monitor, System Controller, and VHS Recorder.

from the system controller is recorded directly on the recorder and viewed constantly on the TV monitor. The system set up is shown in Figure 9.

5. Welding Equipment

The power source of the welding arc was a Miller Model SR600/SCMIA 230/450 Volts. The heart of the welding system, the power source, can be set at different currents that range from 50 to 500 amps and a voltage range of 10 to 35 volts.

Figure 10. Miller Welding Equipment.

Figure 10 shows the Miller welding equipment. Part of the welding system is the torch that is water cooled and capable of heavy duty welding up to 600 A. The torch is designed to

firmly hold the tungsten electrode and to transmit the welding current to the electrode. A ceramic nozzle at the end of the torch is used to shield the inert shielding gas around the electrode. Argon was used as the shielding gas. Figure 11 is the system set up for the GTAW torch and associated electric cables and water connection.

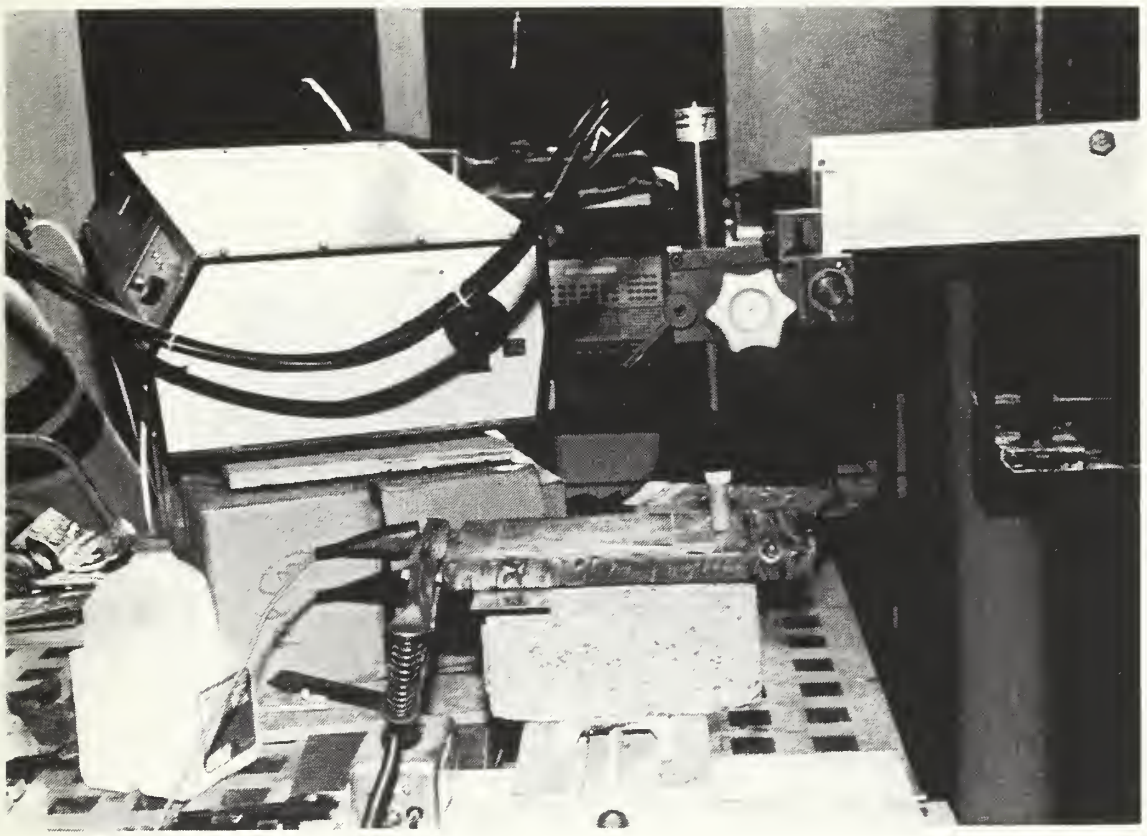

Figure 11. GTAW Torch Setup for Automatic Welding.

D. EXPERIMENTAL PROCEDURE

The welding samples were rectangular HY-80 plates 2.54 cm (1 inch) thick with dimensions of 15.24 by 30.48 cm (6 by 12 inches) as shown in Figure 12. On the upper surfaces of the plates were seven small grooves 38.1 mm (1.5 inches) apart made to simulate butt welding. The length of each groove was 152.4 mm (6 inches) with a width and depth of 1.5875 mm (1/16 inch). The experiments were conducted at varying current levels and welding speeds. There were four nominal current

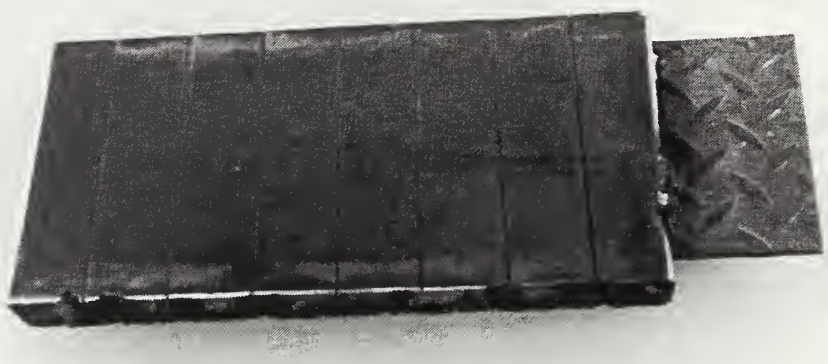

Figure 12. HY-80 Steel Plate 2.54 cm Thick.

settings of 240, 200, 175, and 150 Amps and three welding speeds of 2.117 mm/sec (5 in/min), 1.693 mm/sec (4 in/min), and 1.269 mm/sec (3 in/min). The welding current and voltage were measured with a Digi-Meter 600 Miller Style No. JK-32. The current readings during each experiment fluctuated within ± 5 Amps and the voltage varied from ± .2 Volts. The arc length and electrode tip angle were maintained the same throughout the experiments at 3 mm and 45 degrees respectively.

Measurements of the weld pool dimensions were made for thirty-six runs. The weld pool video image from the vision system was used to measure the weld pool length ahead and behind the arc. Solidified weld samples were cross sectioned, polished, and etched and then analyzed with the help of optical microscopy to measure the weld pool width and the depth of the fusion zone. These measurements were then used as an input to the numerical model described later. A summary of all the welding settings and weld pool dimensions are tabulated in Tables II to IV. Figures 13 to 15 show the weld pool depth as a function of the power input at various speeds. As expected, at a given speed the higher the power input, the deeper the weld pool depth. Figure 16 shows the collection of such data for the various speeds. It can be seen that at the same power input, increasing weld speed causes a shallower weld pool.

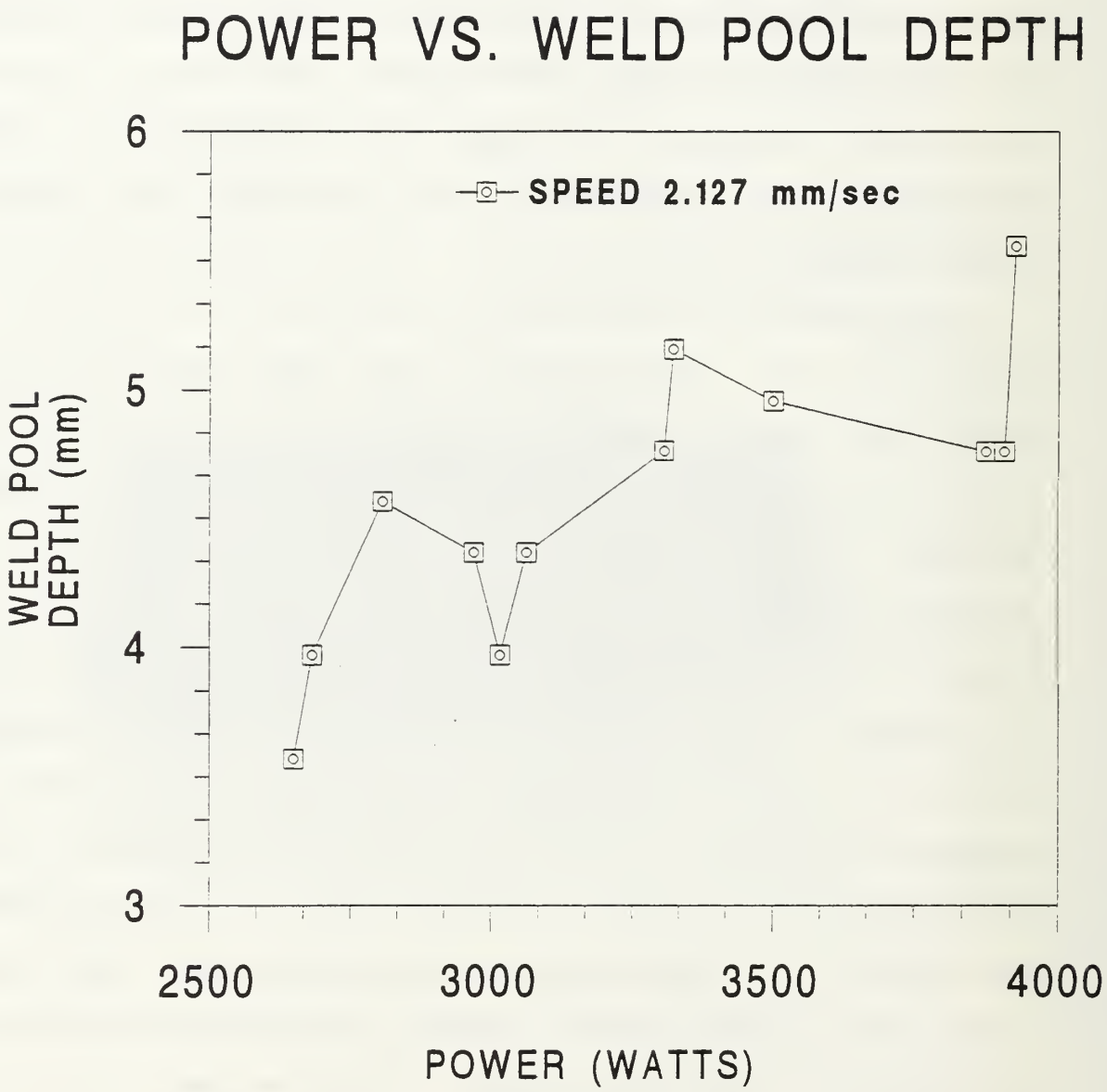

Figure 13. Weld Pool Depth vs Power (Speed 2.127 mm/s).

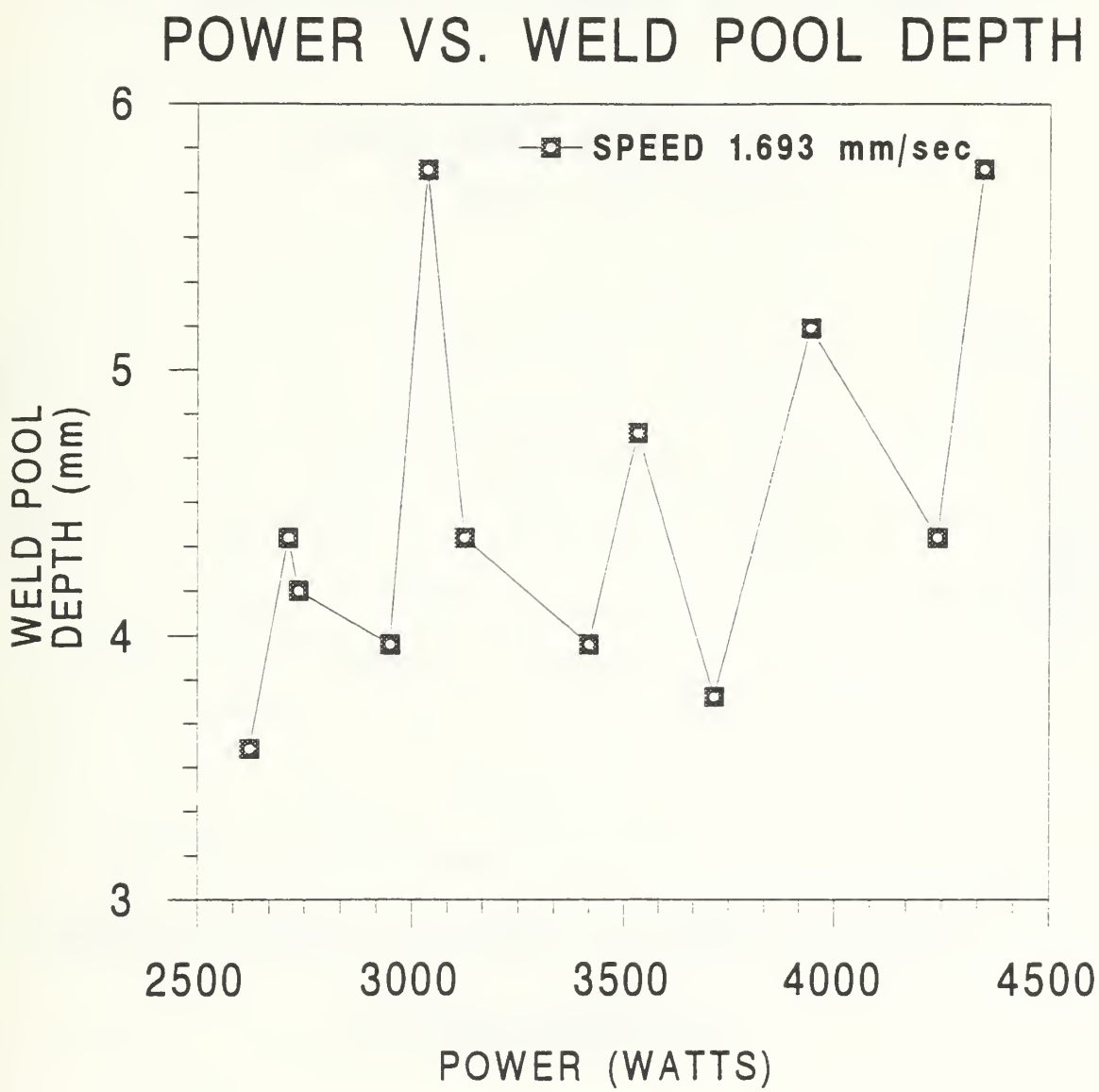

Figure 14. Weld Pool Depth vs Power (Speed = 1.693 mm/s).

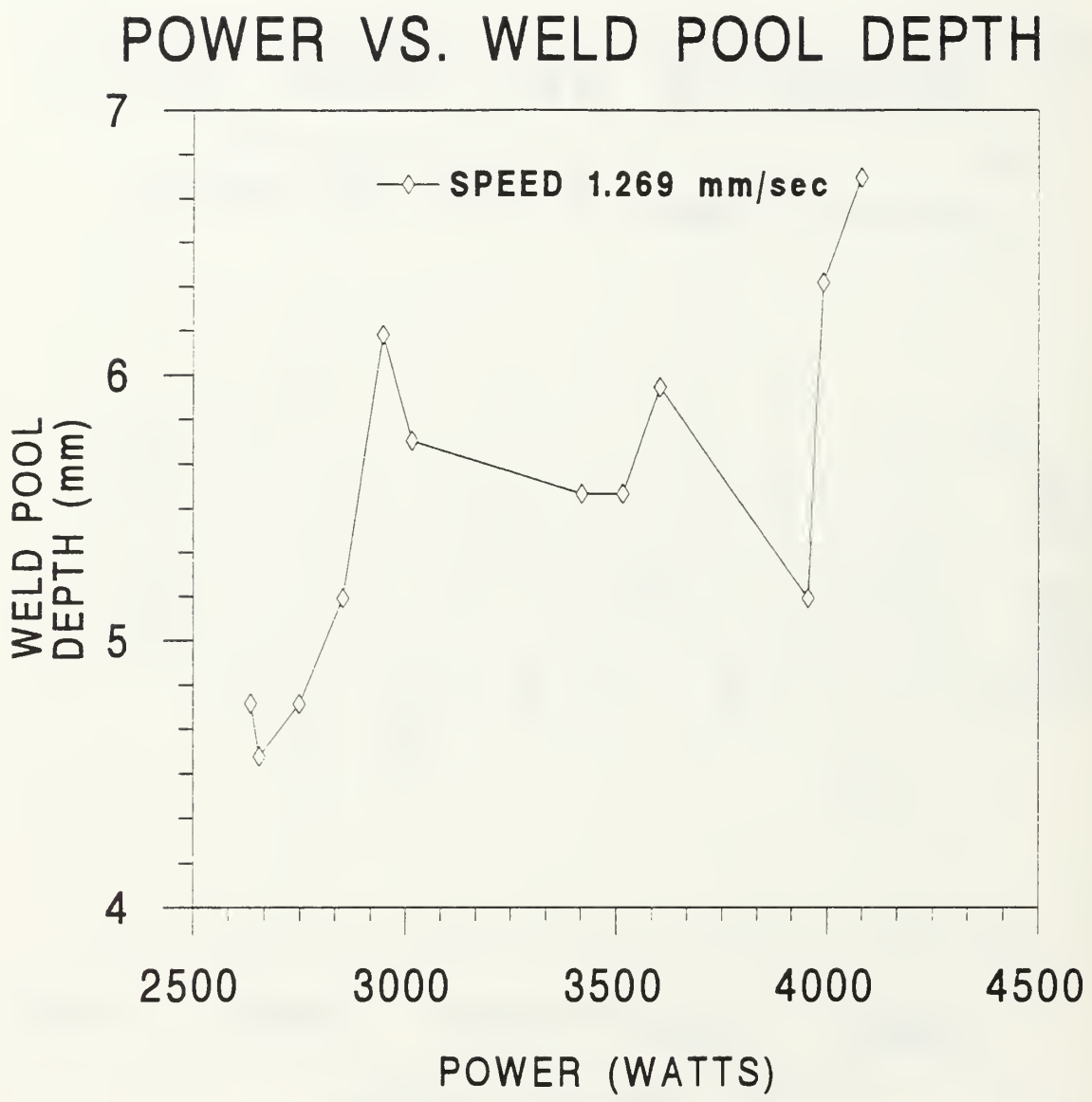

Figure 15. Weld Pool Depth vs Power (Speed = 1.269 mm/s).

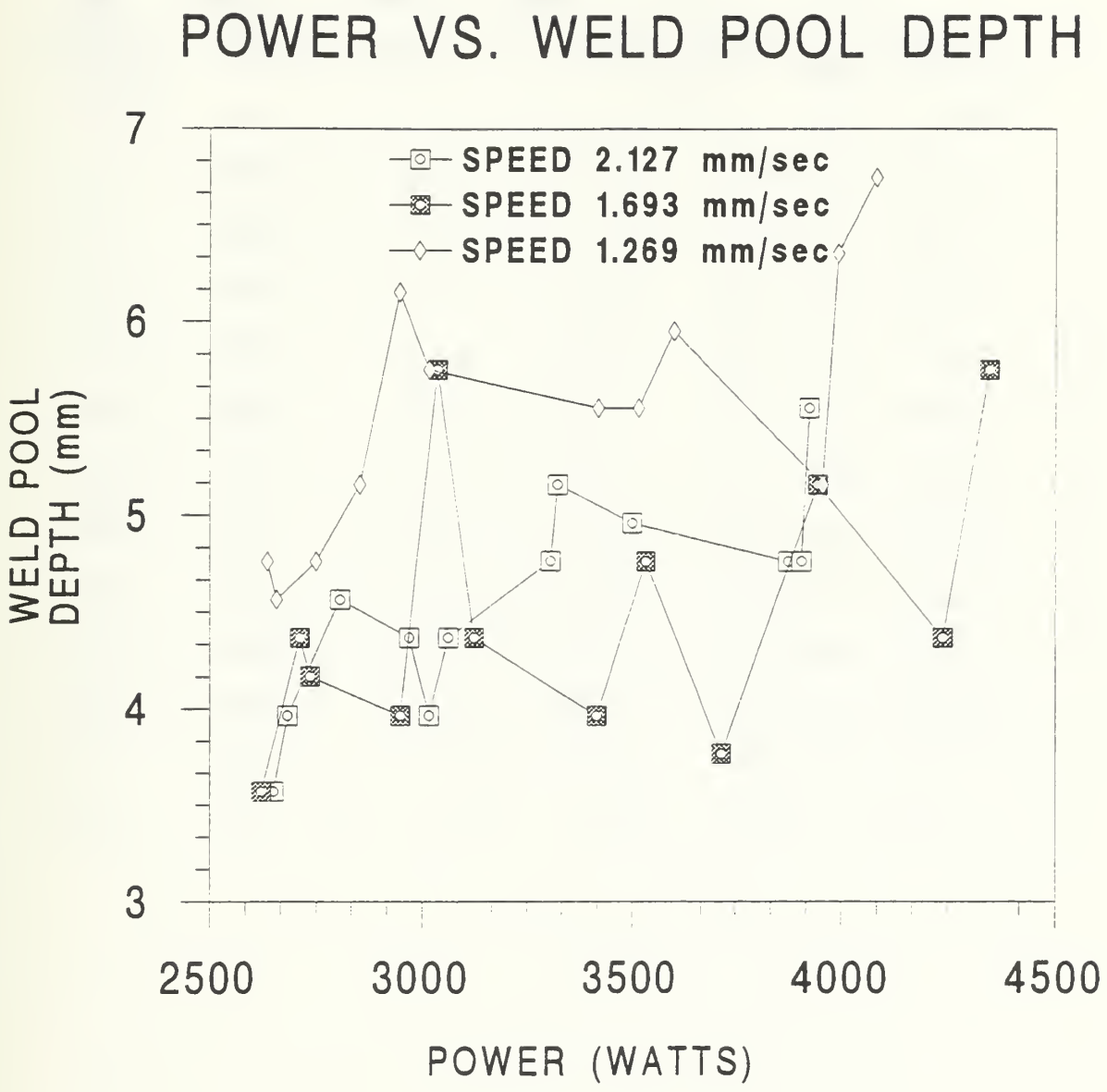

Figure 16. Effect of Power vs Weld Pool Depth at Different Speeds.

Table II. SUMMARY OF WELDING SETTINGS AND WELD POOL MEASUREMENTS WITH SPEED OF 2.127 mm/sec.

Power (Watts)	Amps (±4)	Volts (±.3)	Weld Pool Width (mm)	Weld Pool Depth (mm)	Weld Pool length Ahead (mm)	Behind (mm)
4347.0	315	13.8	10.714	5.754	3.830	9.340
4239.0	314	13.5	13.096	4.365	3.300	12.000
3944.6	326	12.1	10.318	5.159	2.980	10.800
3715.2	288	12.9	11.112	3.770	3.000	9.150
3533.2	292	12.1	10.714	4.762	3.000	9.150
3416.4	292	11.7	10.318	3.968	3.150	8.400
3123.6	274	11.4	7.540	4.365	3.000	6.675
3036.0	264	11.5	7.142	5.754	3.375	4.875
2948.0	268	11.0	8.730	3.968	2.625	7.875
2735.9	251	10.9	7.142	4.167	3.150	6.375
2710.4	242	11.3	7.963	4.365	2.625	6.375
2621.5	245	10.7	7.540	3.571	2.475	6.900

Table III. SUMMARY OF WELDING SETTINGS AND WELD POOL MEASUREMENTS WITH SPEED OF 1.693 mm/sec.

Power length Behind (mm)	Amps (Watts)	Volts (±4)	Weld Pool (±.3)	Weld Pool Width (mm)	Weld Pool Depth (mm)	Weld Pool Ahead (mm)
3925.0	314	12.5	7.936	5.556	3.110	8.110
3906.0	315	12.4	9.525	4.762	3.050	7.500
3874.5	315	12.3	8.730	4.762	2.560	7.627
3500.0	280	12.5	7.142	4.960	2.810	7.380
3322.8	284	11.7	8.334	5.159	2.740	7.440
3306.0	285	11.6	7.142	4.764	2.680	7.930
3062.4	264	11.6	7.142	4.365	2.440	7.200
3016.0	260	11.6	8.334	3.968	2.560	6.220
2969.0	256	11.6	7.142	4.365	2.800	6.770
2806.0	244	11.5	7.142	4.564	2.620	6.580
2681.4	246	10.9	7.142	3.968	2.440	5.490
2648.7	243	10.9	7.142	3.571	2.500	5.980

Table IV. SUMMARY OF WELDING SETTINGS AND WELD POOL MEASUREMENTS WITH SPEED OF 1.269 mm/sec.

Power length Behind (mm)	Amps (Watts)	Volts (±4)	Weld Pool (±.3)	Weld Pool Width (mm)	Weld Pool Depth (mm)	Weld Pool Ahead (mm)
4082.0	314	13.0	10.318	6.746	3.554	6.800
3992.8	322	12.4	10.318	6.350	3.700	7.110
3955.6	319	12.4	10.318	5.159	3.000	9.750
3602.5	275	13.1	11.112	5.953	4.300	10.100
3517.9	277	12.7	11.112	5.556	4.000	10.580
3420.0	285	12.0	11.112	5.556	4.000	10.460
3016.0	260	11.6	7.936	5.754	3.690	5.530
2946.4	254	11.6	9.525	6.151	3.477	7.620
2852.7	257	11.1	9.920	5.159	3.960	8.050
2749.2	237	11.6	6.746	4.762	3.780	7.200
2656.8	246	10.8	6.350	4.564	3.350	6.100
2635.2	244	10.8	7.936	4.763	3.477	6.220

III. COMPUTATIONS OF WELDING EFFICIENCY

This chapter describes the numerical method used to estimate the net heat transfer rate to the workpiece, under quasi-steady conditions, for a given shape and size of the weld pool. The formulation and computations are done in a reference frame that moves with the welding torch. In this moving coordinate system, the heat transfer is quasi-steady since the weld pool location, shape, size, and the temperature distribution in the workpiece, remain invariant with respect to the torch. Under this assumption, the heat input from the heat source to the weld pool is equal to the net heat transfer from the weld pool boundary to the workpiece. If we prescribe the weld pool shape and size (based on experimental data) and set the weld pool boundary at the melting temperature T_m, the resulting heat transfer across the weld pool boundary can be estimated by solving the temperature distribution in the workpiece due to conduction.

The weld pool shape is assumed to be that of a double ellipsoid. Such a weld pool shape with a corresponding heat source distribution was also assumed by Goldak et al. [Ref. 17]. As shown in Figure 2 in Chapter 1, the four dimensional values (i.e., lengths forward (a_1) and behind the arc (a_2), weld pool width (b), and weld pool depth (c) are needed for each weld pool. These values are obtained from the

experimental runs as described in the previous chapter. The weld pool depth and width were measured by analyzing a weld section using optical microscopy, while the half-lengths of the ellipsoid were measured from the corresponding video frames.

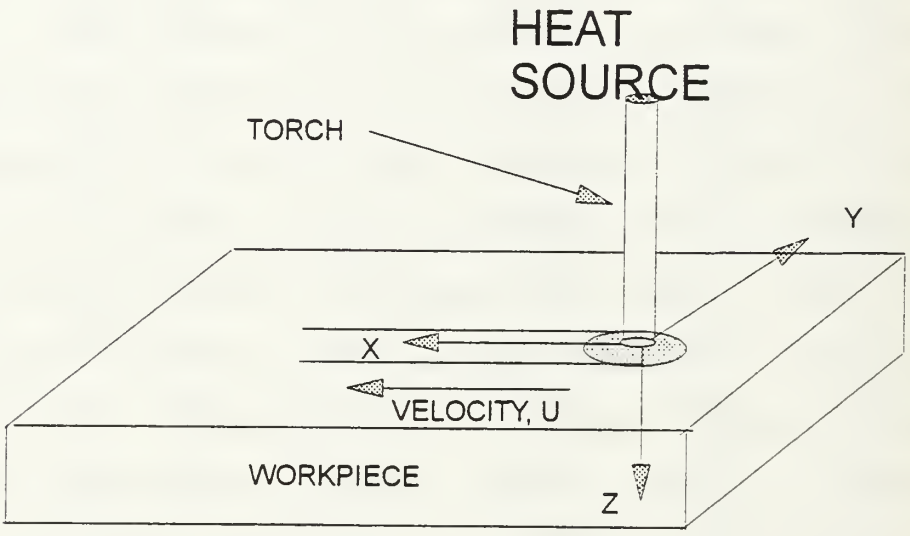

Figure 17. Gas Tungsten Arc Welding (GTAW) Process Showing the Reference and Moving Coordinate System.

A. FORMULATION OF GOVERNING EQUATIONS

The temperature distribution in the solid region outside the fusion zone is described by:

$$\frac{\partial}{\partial t}(\rho T) = \frac{\partial}{\partial x'}\left(\frac{k}{C_p}\frac{\partial T}{\partial x'}\right) + \frac{\partial}{\partial y}\left(\frac{k}{C_p}\frac{\partial T}{\partial y}\right) + \frac{\partial}{\partial z}\left(\frac{k}{C_p}\frac{\partial T}{\partial z}\right) + Source \qquad Eq\ (1)$$

where x', y, z are the coordinates in the stationary reference frame. We introduce the following coordinate transformation

$$x = x' - U_{torch}t \qquad Eq\ (2)$$

where U_{torch} is the velocity of the torch (a constant). Differentiating Eq (2) with respect to time,

$$\frac{\partial x}{\partial t} = \frac{\partial x'}{\partial t} - U_{torch}$$

or,

$$U = U' - U_{torch} \qquad Eq\ (3)$$

where U is the velocity in the x direction in the moving reference frame. For any general variable Φ, applying the chain rule to the x'- directional differential term yields:

$$\frac{\partial}{\partial x'}(\phi(x', y, z, t)) = \frac{\partial x}{\partial x'}\frac{\partial}{\partial x}(\phi(x, y, z, t))$$

$$= \frac{\partial}{\partial x}(\phi(x, y, z, t)) \qquad Eq\ (4)$$

$$\frac{\partial}{\partial x'}\left(\frac{\partial}{\partial x'}(\phi(x', y, z, t))\right) = \frac{\partial}{\partial x}\left(\frac{\partial}{\partial x}(\phi(x, y, z, t))\right) \qquad Eq\ (5)$$

$$\frac{\partial}{\partial t}(\phi(x',y,z,t)) = \frac{\partial}{\partial t}(\phi(x,y,z,t)) + \frac{\partial x}{\partial t}\frac{\partial}{\partial x}(\phi(x,y,z,t))$$

$$= \frac{\partial}{\partial t}(\phi(x,y,z,t)) + (u' - U_{torch})\frac{\partial}{\partial x}(\phi(x,y,z,t)) \qquad Eq\ (6)$$

Substitution of EQ. (4), (5), and (6) in (1) yields the transformed equation in the reference frame of the moving torch:

$$\frac{d}{\partial t}(\rho T) + \frac{d}{\partial x}(-\rho U_{torch} T) = \frac{d}{\partial x}\left(\frac{k}{C_p}\frac{dT}{\partial x}\right) + \frac{d}{\partial y}\left(\frac{k}{C_p}\frac{dT}{\partial y}\right) + \frac{d}{\partial z}\left(\frac{k}{C_p}\frac{dT}{\partial z}\right) \quad Eq(7$$

B. BOUNDARY CONDITIONS

The boundary conditions are as follows:

Convective boundary condition on the sides, and top:

$$z=0; \quad h(T_f - T) = -k\frac{\partial T}{\partial z}$$

$$z=z_L; \quad h(T_f - T) = k\frac{\partial T}{\partial z}$$

$$x=0; \quad h(T_f - T) = -k\frac{\partial T}{\partial x}$$

$$x=x_L; \quad h(T_f-T)=k\frac{\partial T}{\partial x}$$

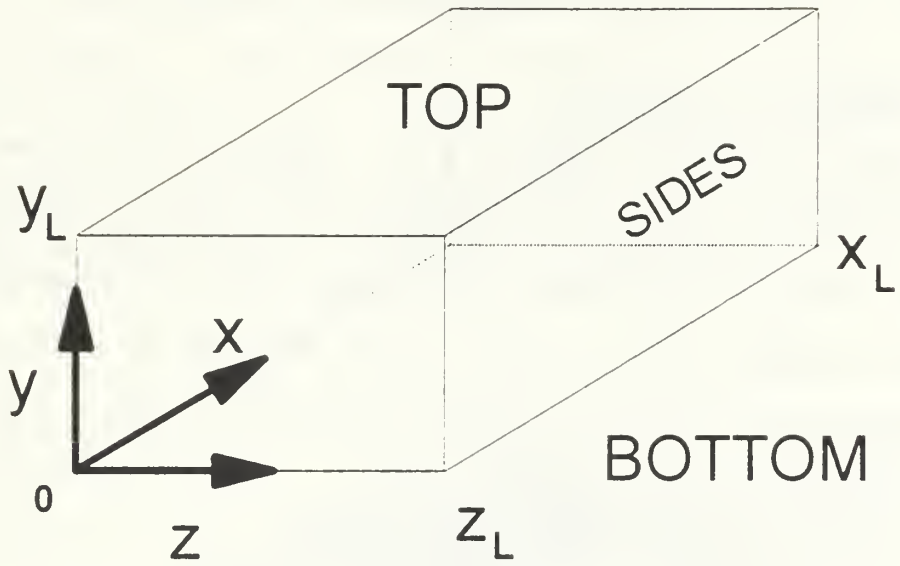

Top:

$$y=y_L; \quad h(T-T_f)+\epsilon\sigma(T^4-T_f^4)=-k\frac{\partial T}{\partial y}$$

Bottom (Insulated):

$$y=0; \quad \frac{\partial T}{\partial y}=0$$

At the weld pool boundary and its interior: $T = T_m$

where:

h = heat transfer coefficient

T_f= ambient fluid temperature

ϵ = emissivity

σ = Stefan Boltzman constant

k = thermal conductivity of the solid

T_m= melting temperature of the solid

C. NUMERICAL SOLUTION

The governing equation (8), together with the boundary conditions are then solved numerically using a control-volume based finite difference technique. Since our problem is a quasi-steady one, and the finite difference code used is a transient one, iterations were continued until a steady state

Table V. PHYSICAL PROPERTIES OF HY-80.

Density, ρ	7800 kg/m^3
Thermal Conductivity, K	35 W/m-K
Heat Capacity, C_p	Figure 19
Melting Temperature, T_{melt}	1477^0 C
Ambient Temperature, T_{amb}	25^0 C

condition was reached. The rectangular domain was discretized into a fine mesh grading as shown in Figure 18. The grading near the heat source is on the order of .5 mm by .5 mm by .5 mm. Outside the heat source, a non-uniform grid is employed. A Silicon Graphics Iris workstation was used for the computations. The physical dimensions used are shown in Tables II, III, and IV. In the computations the specific heat is assumed to vary with temperature as seen in Figure 19. The thermal conductivity, as shown in Figure 20,

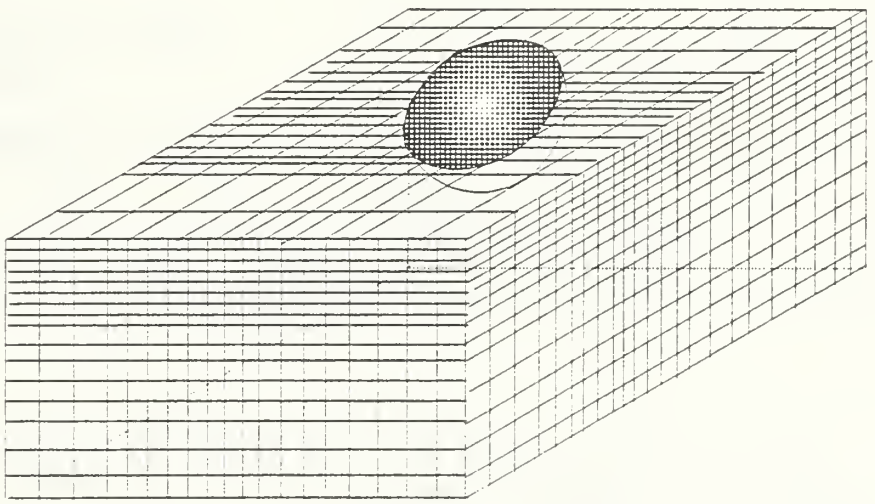

Figure 18. Grid Network used in the Computations.

does not seem to vary appreciably over the temperature range of our operation and is therefore assumed to be constant at 35 W/m-k. Other pertinent data used are tabulated in Table V.

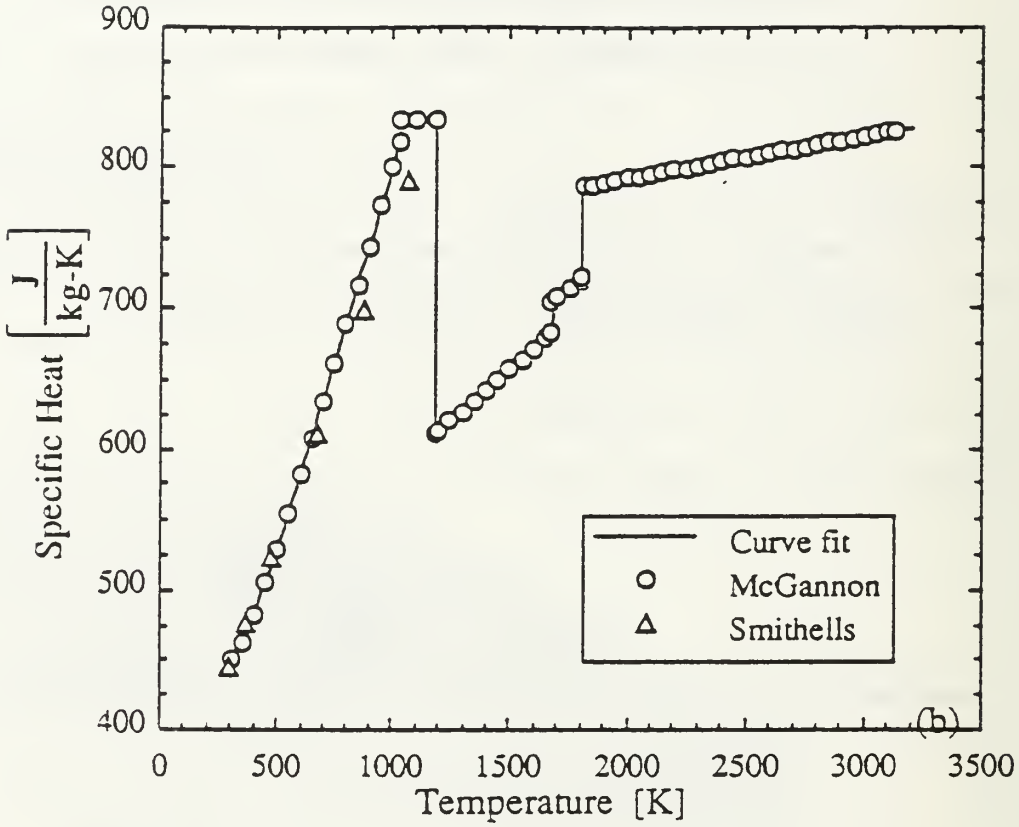

Figure 19. Specific Heat as a Function of Temperature for Iron [Ref. 21].

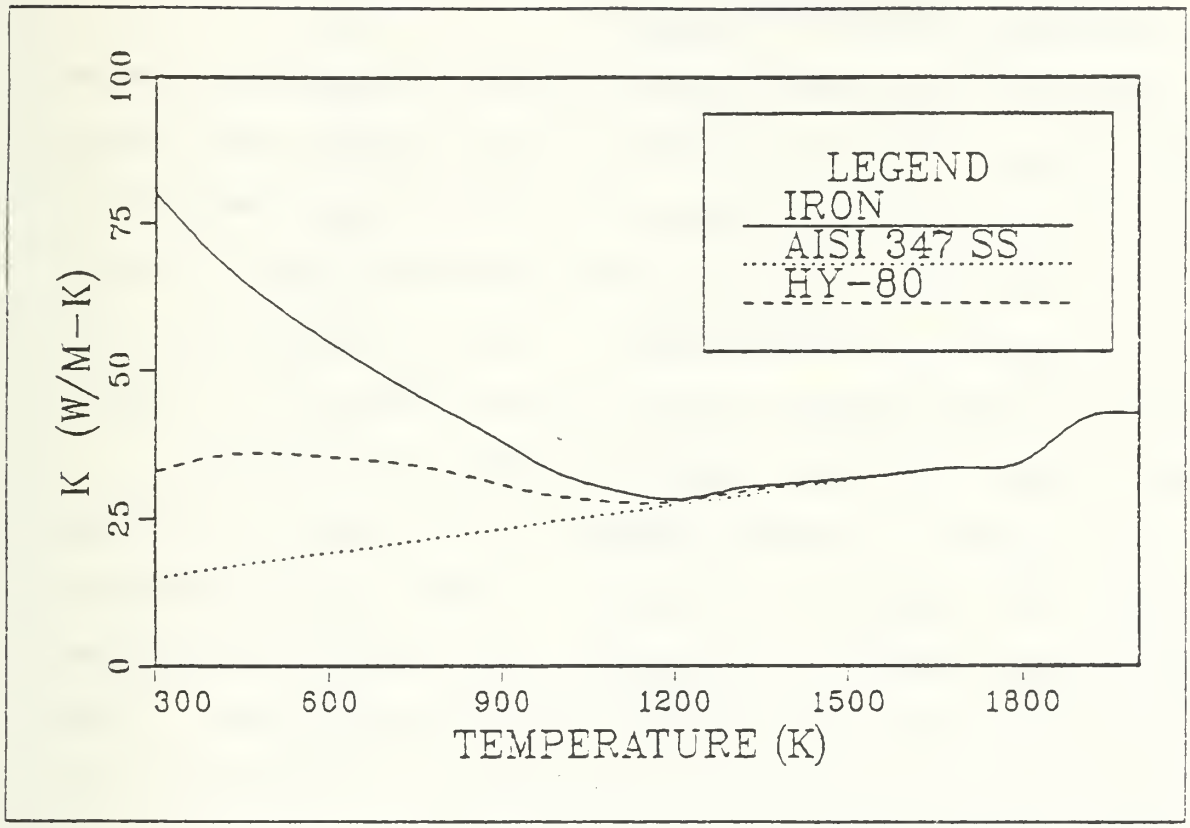

Figure 20. Thermal Conductivity vs Temperature of Iron Based Alloy [Ref. 22].

IV. RESULTS AND DISCUSSION

A. ESTIMATING WELDING EFFICIENCY

Results of the GTAW efficiency made on HY-80 plates were tabulated to compare the effects of the varying input power set at high, medium, and low. The power inputs ranged from 4.347 to 2.621 KW. Three different speed settings were used for the moving arc experiments. Table VI summarizes the efficiency measurements for the welding speed of 2.12 mm/s, Table VII for 1.69 mm/s, and Table VIII for 1.269 mm/s.

An increase in current caused the efficiency to decrease as seen in Figures 21 to 23. Based on calorimetric measurements, Giedt et al [Ref. 15] reported an average efficiency of 80% for welding 304L stainless steel. They compared their results with other studies on GTAW efficiency determination using temperature field measurements. The currents ranged from 40 to 200 amps and a decreasing trend was found for the efficiencies with increasing currents. Present experiments were conducted at higher currents ranging from 237 to 326 Amps and the measured efficiencies ranged from 62 to 84%. These values fall within the range reported in previous studies.

Table VI. SUMMARY OF GTA WELDING EFFICIENCY MEASUREMENTS WITH SPEED 2.127 mm/sec.

Run #	Input Power (W)	Total Heat Input (W)	Efficiency (%)
1	3925	2590	66
2	3906	2601	67
3	3875	2407	62
4	3500	2289	65
5	3323	2471	74
6	3306	2241	68
7	3062	2080	68
8	3016	2092	69
9	2969	2115	71
10	2806	2116	75
11	2181	1888	70
12	2649	1864	70

Table VII. SUMMARY OF GTA WELD EFFICIENCY MEASUREMENTS WITH WELDING SPEED OF 1.693 mm/sec.

Run #	Input Power (W)	Total Heat Input (W)	Efficiency (%)
13	4347	2849	66
14	4239	3084	73
15	3945	2846	72
16	3715	2518	68
17	3533	2702	76
18	3416	2448	72
19	3124	2123	68
20	3036	2230	73
21	2948	2191	74
22	2731	2029	74
23	2710	2101	78
24	2622	1894	72

Table VIII. SUMMARY OF GTA WELD EFFICIENCY MEASUREMENTS WITH WELDING SPEED OF 1.269 mm/sec.

Run #	Input Power (J)	Total Heat Input (W)	Efficiency (%)
25	4082	2542	62
26	3993	2525	63
27	3956	2638	67
28	3603	2672	74
29	3518	2716	77
30	3420	2710	79
31	3016	2202	73
32	2946	2503	85
33	2853	2420	85
34	2749	2031	74
35	2657	1923	72
36	2635	2115	80

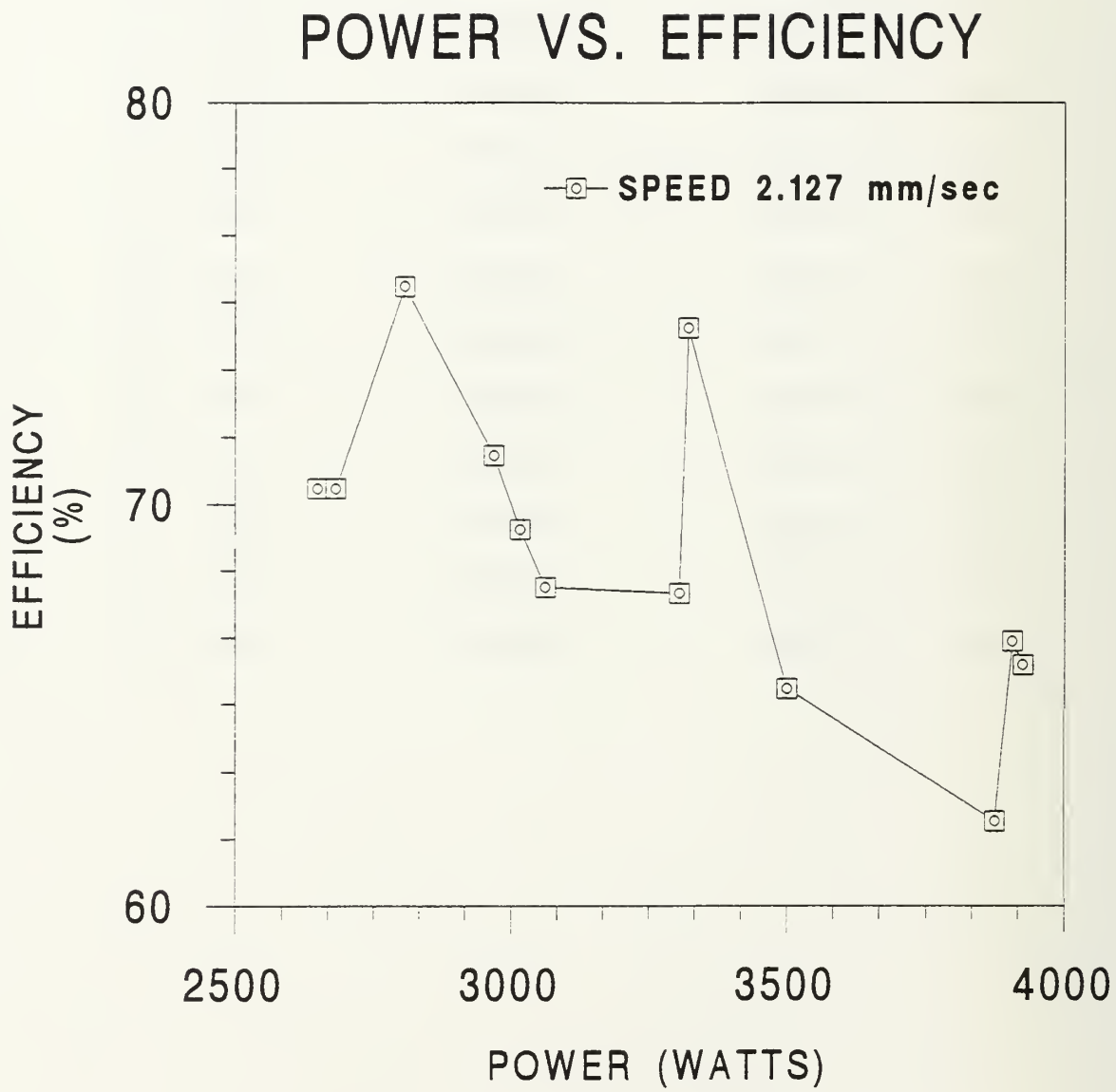

Figure 21. Effect of Power vs Efficiency at Speed of 2.127 mm/sec.

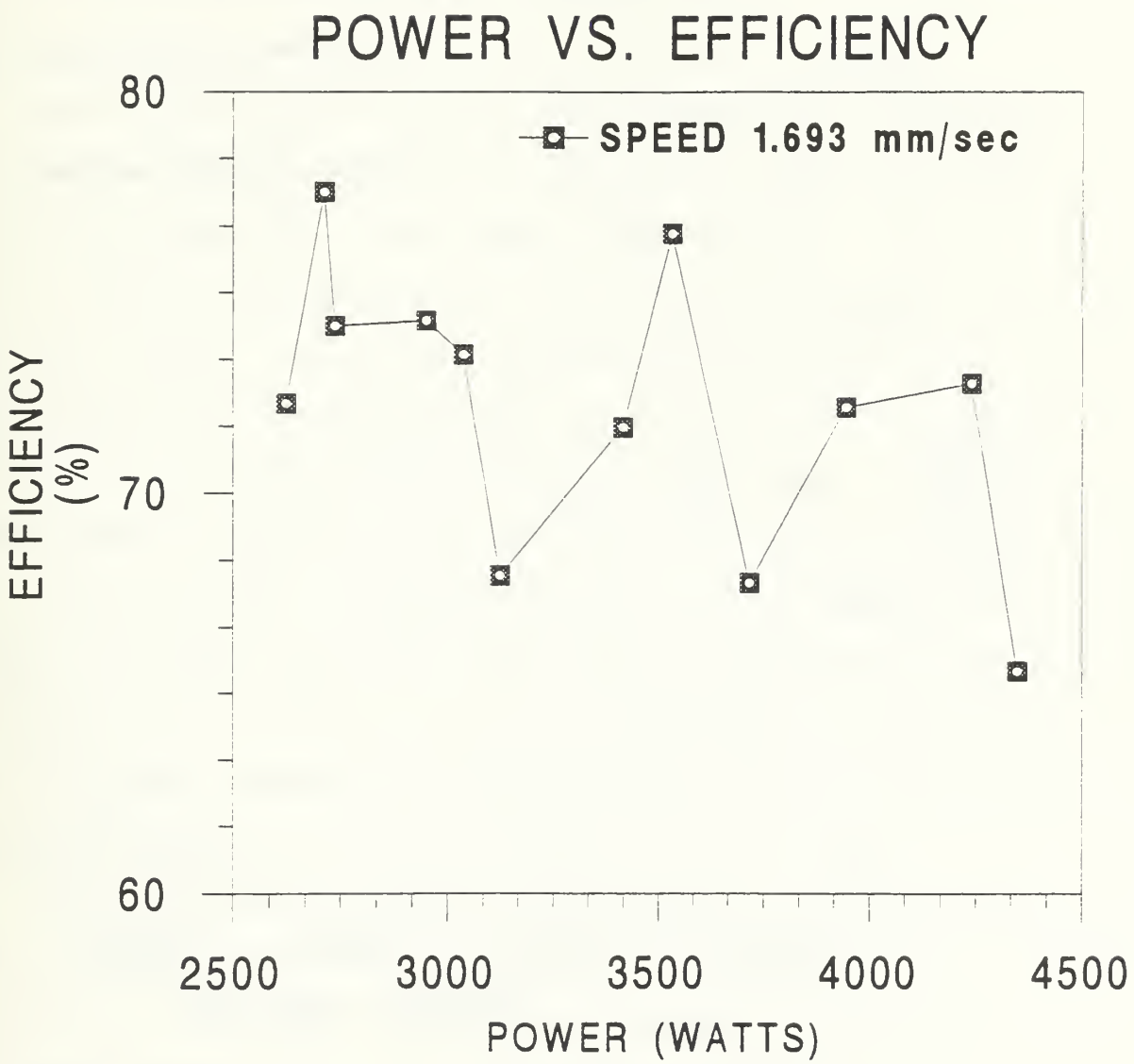

Figure 22. Effect of Power vs Efficiency at Speed of 1.693 mm/sec.

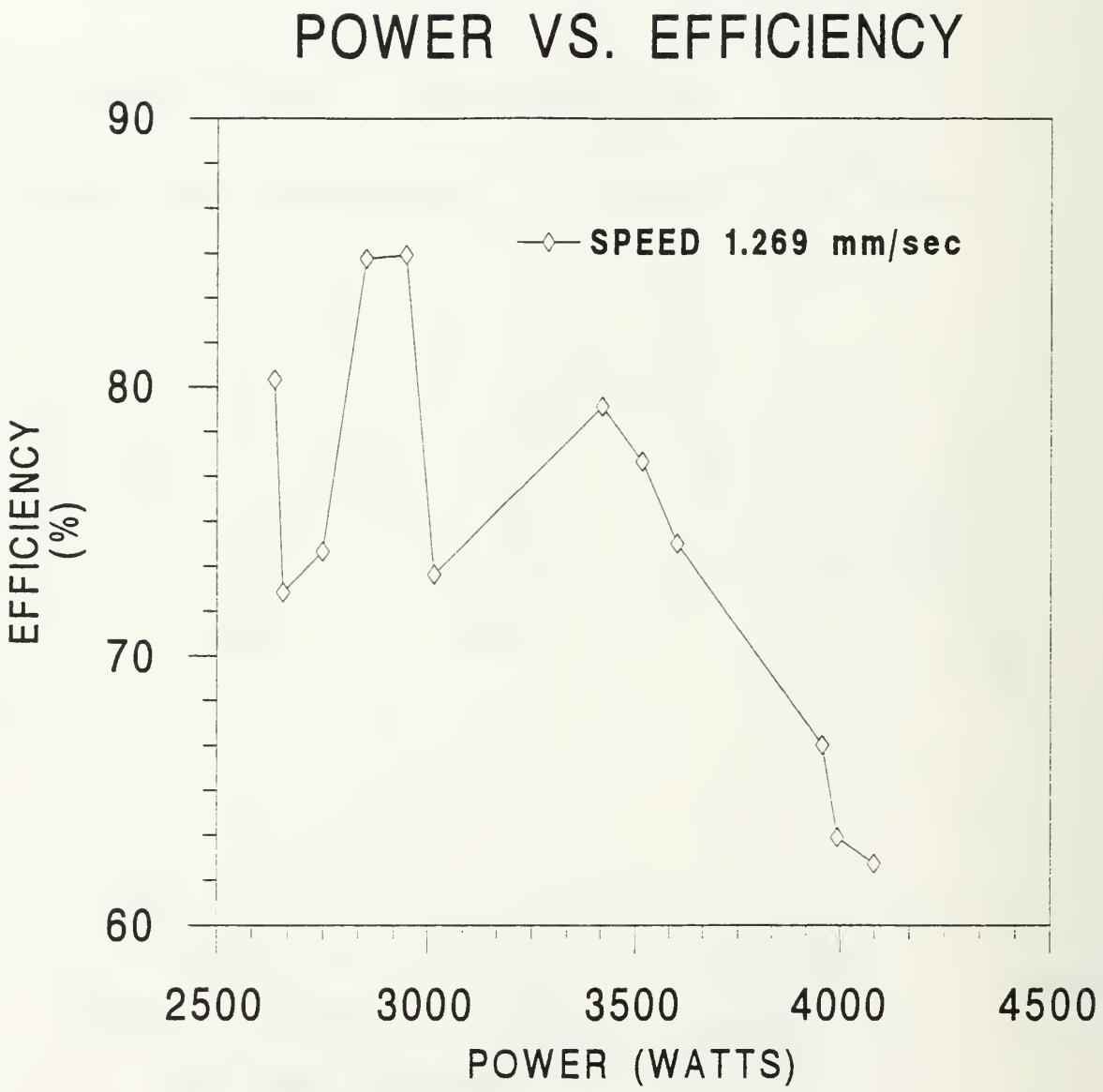

Figure 23. Effect of Power vs Efficiency at Speed of 1.269 mm/sec.

Apparently, at higher power inputs more heat loss to the surroundings due to radiation and convection results in lower efficiencies. Welding speed also influences the efficiencies. As noted in Figure 24, the slower the speed, the higher the efficiencies.

B. TEMPERATURE CONTOURS

Based on the heat conduction model developed, the effects of the power input and torch speed on the temperature field outside the weld pool were computed and plotted. Figures 25 to 33 exhibits selected results for nine weld pool geometries. For each figure, (a) is the calculated temperature field at longitudinal section of weld pool, (b) calculated temperature field at traverse section of the weld pool, and (c) experimental composite section of the HY-80 showing the depth of the fusion zone. Figure 34 shows the free surface of a single digitized weld pool video frame, each associated in Figures 25 to 33 with (a) to (i), respectively. The double ellipsoid model appears to be satisfactory in prescribing the weld pool shape.

Figure 35 show the transient development of the weld pool at one second intervals following the arc initiation for a period of 12 seconds. After twelve seconds the weld pool is at quasi-steady state for which the present computational model is accurate. Notice that initially the weld pool is elongated compared to the quasi-steady weld pool size. The

reason behind this is that near the edge, heat transfer from the source is not as efficient as when the torch moves further away, allowing heat conduction in all directions within the metal.

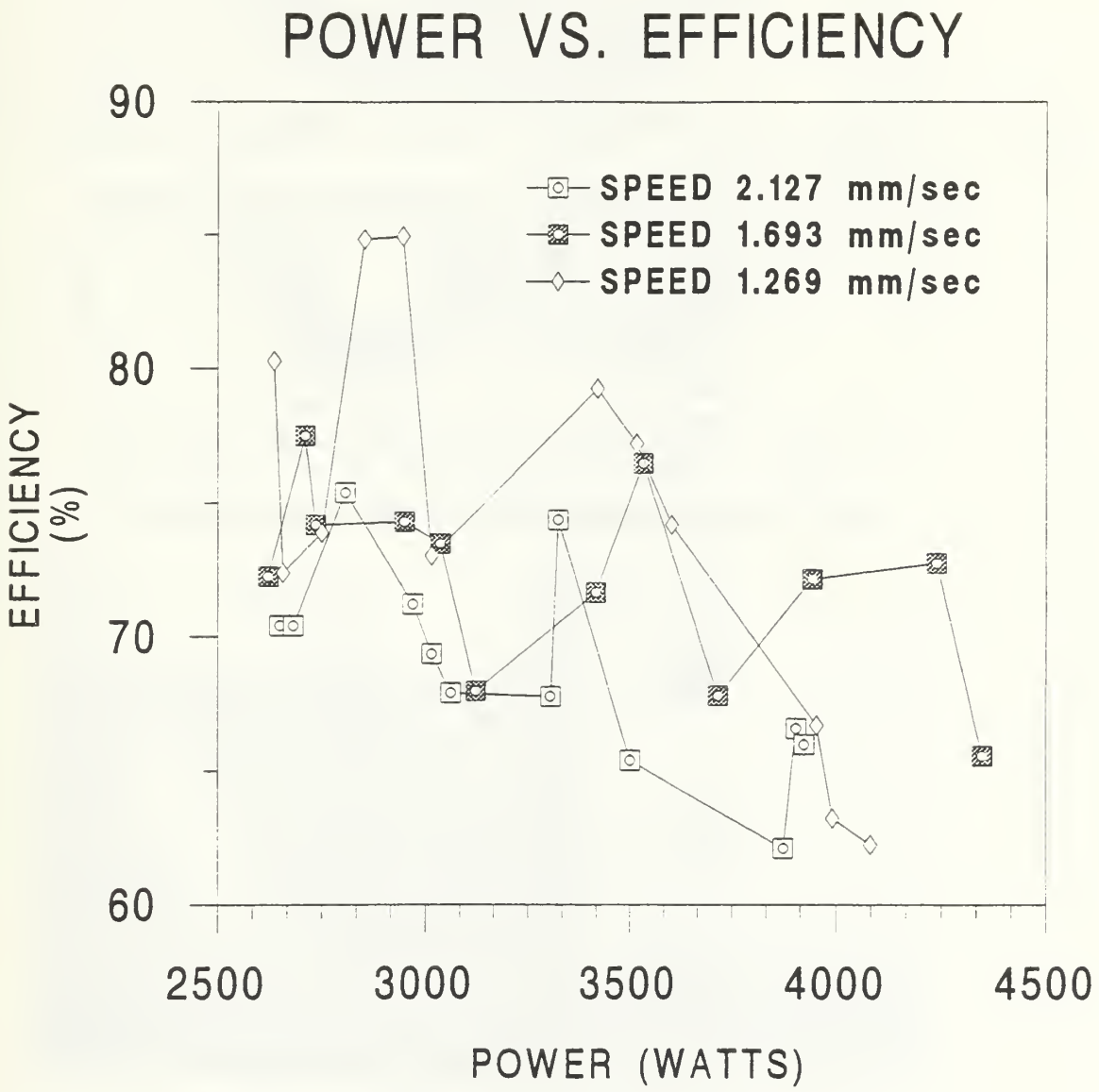

Figure 24. Power vs Efficiency Comparison at Different Speeds.

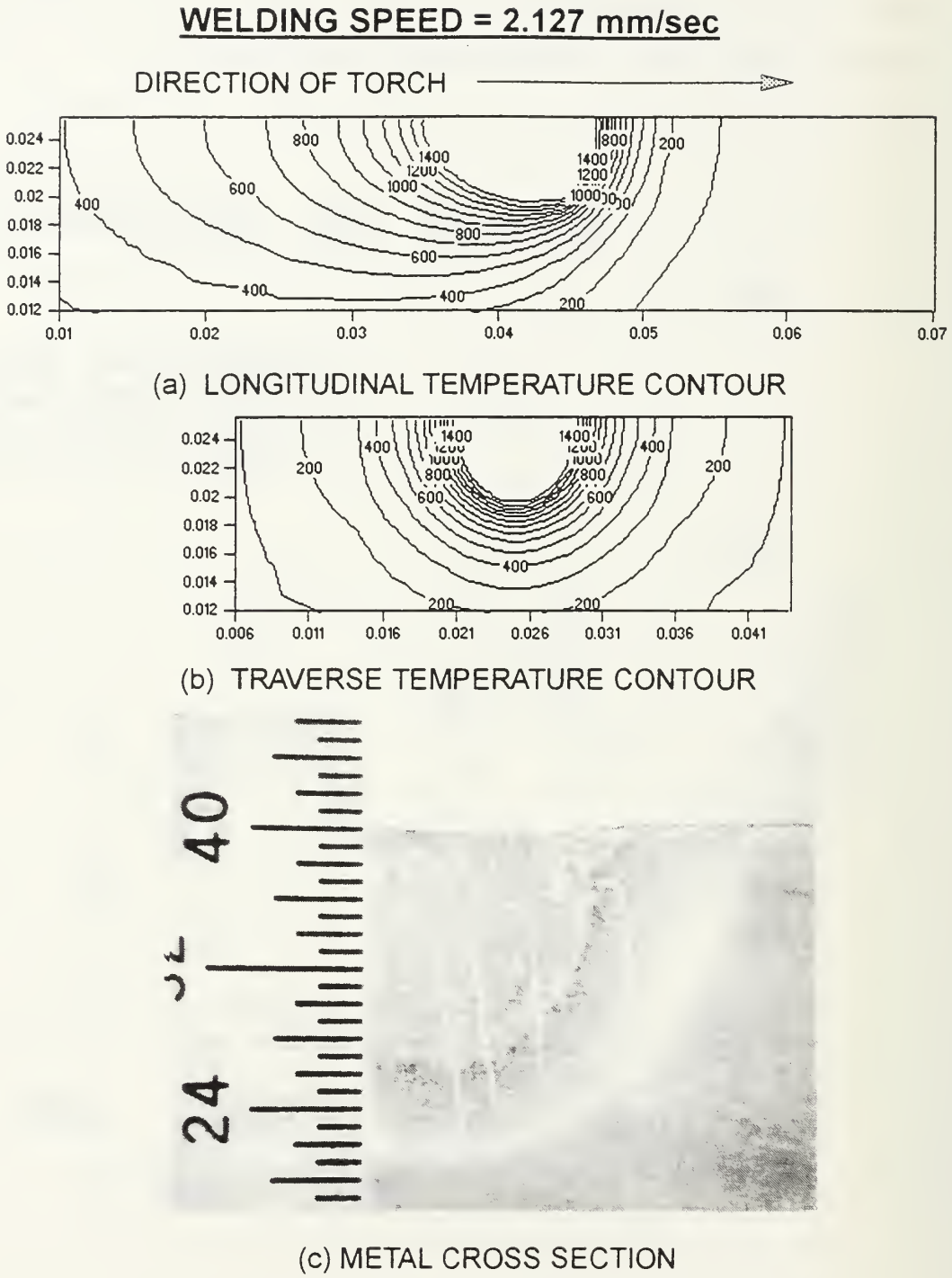

Figure 25. (a) Longitudinal Temperature Contour, (b) Traverse Temperature Contour, and (c) Metal Cross Section for Run #1.

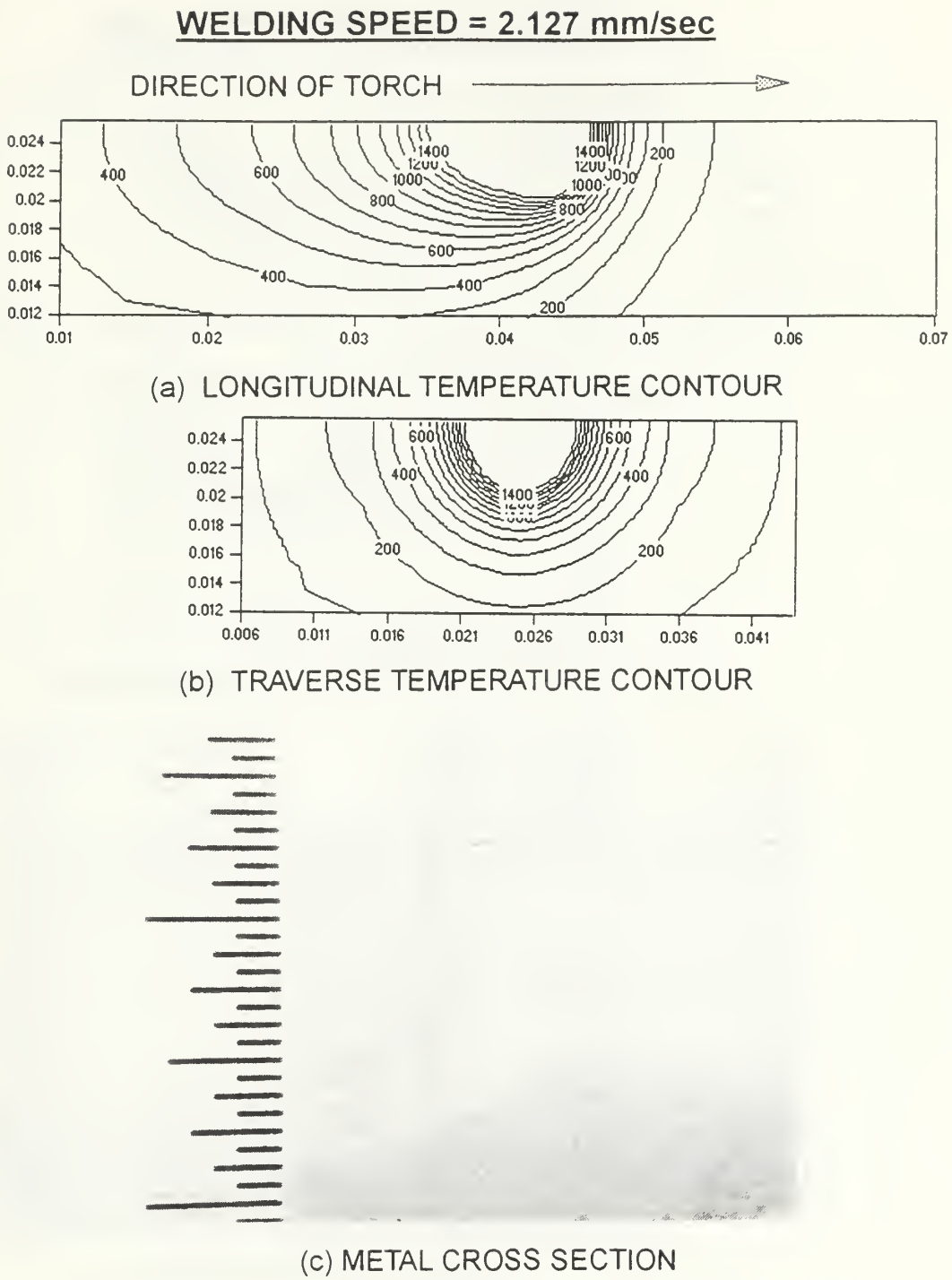

Figure 26. (a) Longitudinal Temperature Contour, (b) Traverse Temperature Contour, and (c) Metal Cross Section for Run #6.

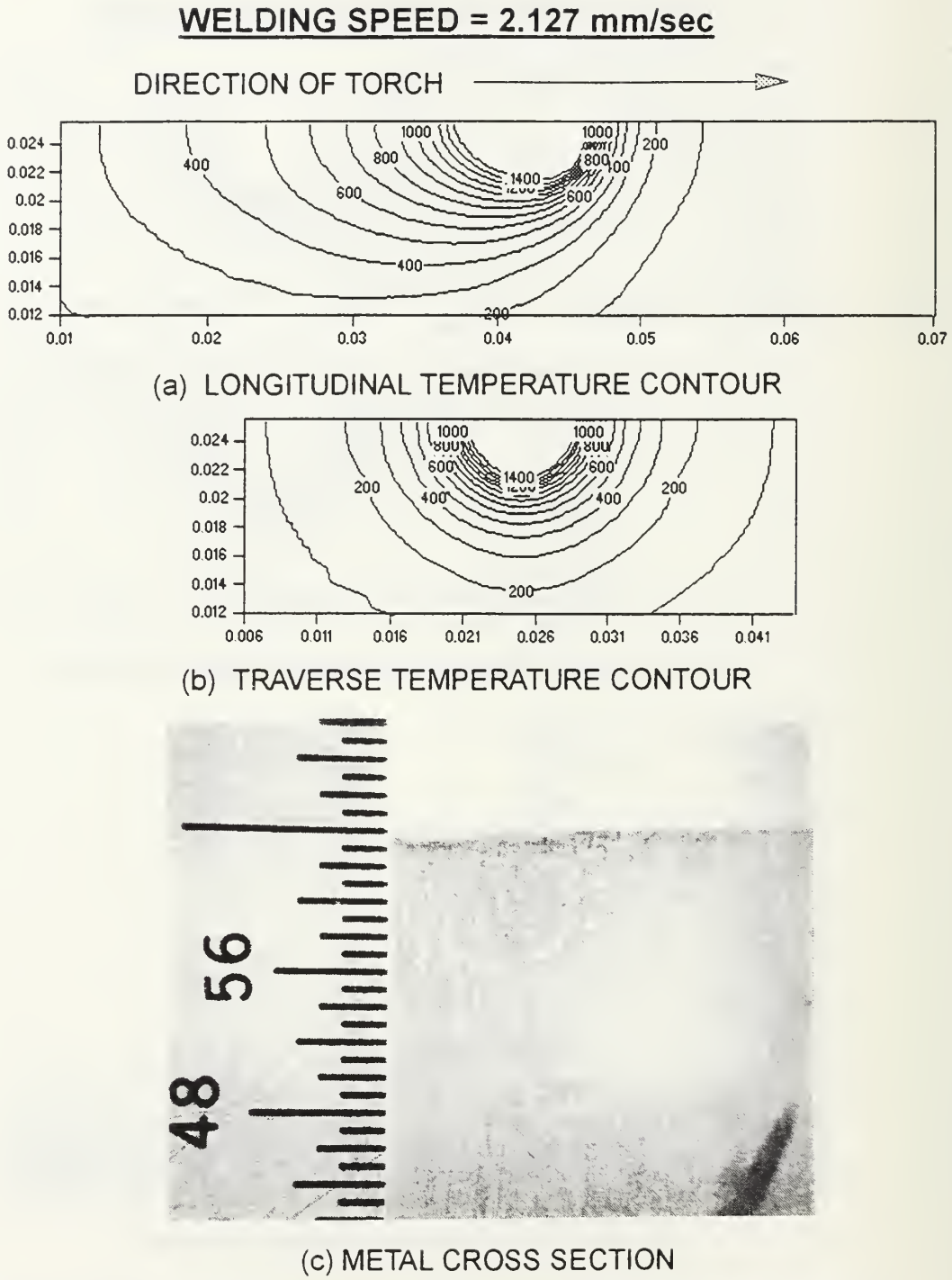

Figure 27. (a) Longitudinal Temperature Contour, (b) Traverse Temperature Contour, and (c) Metal Cross Section for Run #12.

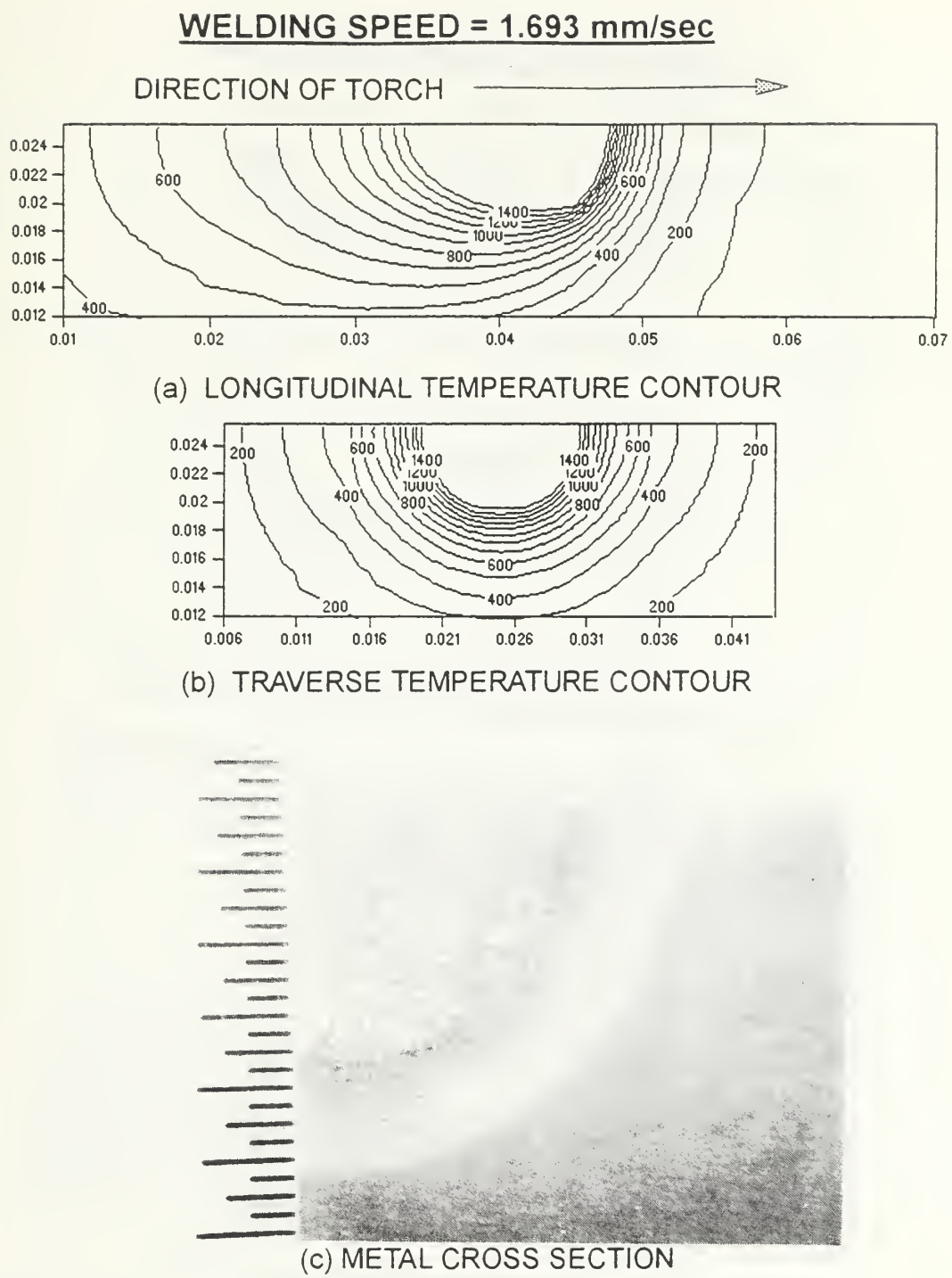

Figure 28. (a) Longitudinal Temperature Contour, (b) Traverse Temperature Contour, and (c) Metal Cross Section for Run #13.

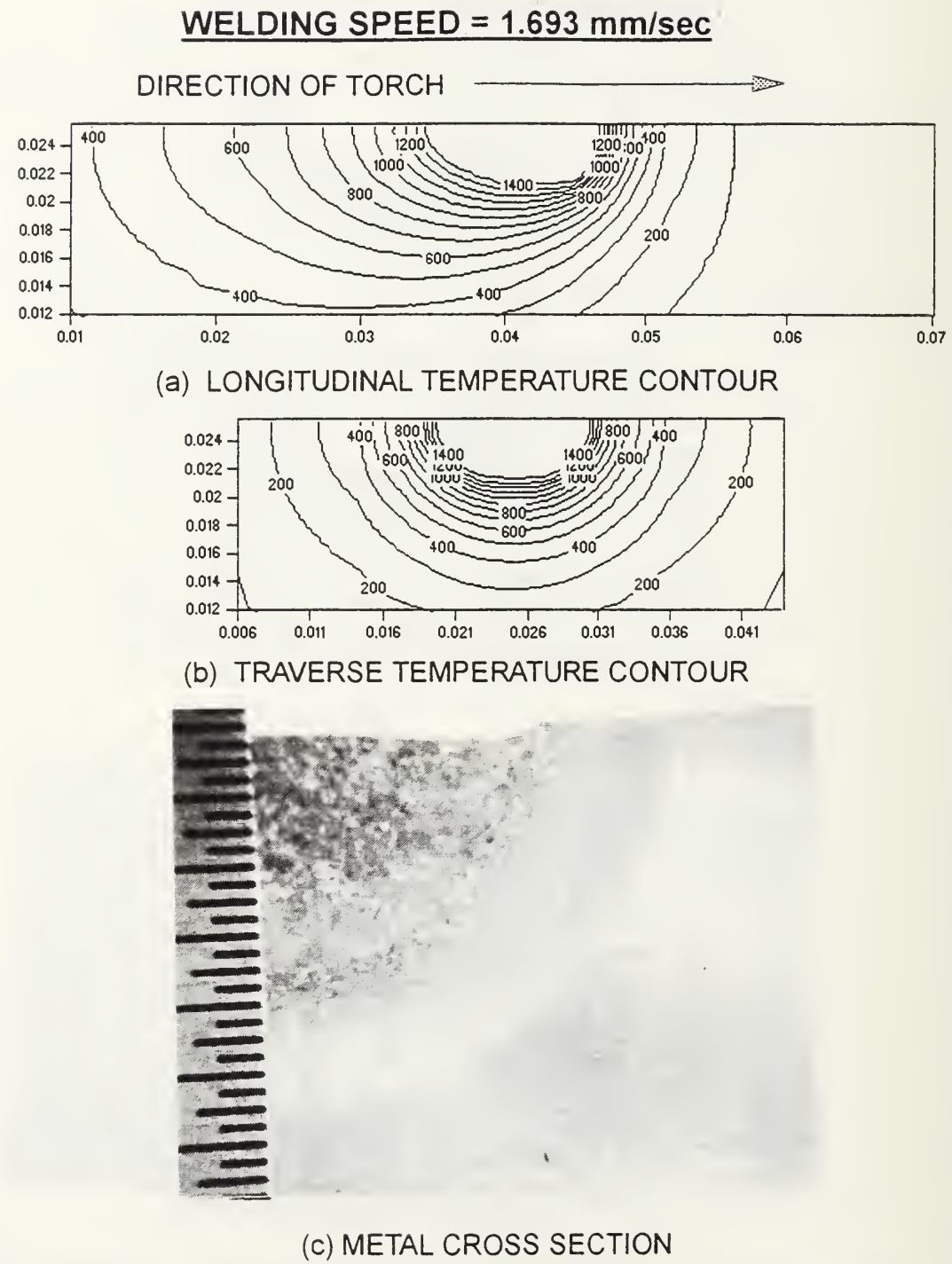

Figure 29. (a) Longitudinal Temperature Contour, (b) Traverse Temperature Contour, and (c) Metal Cross Section for Run #18.

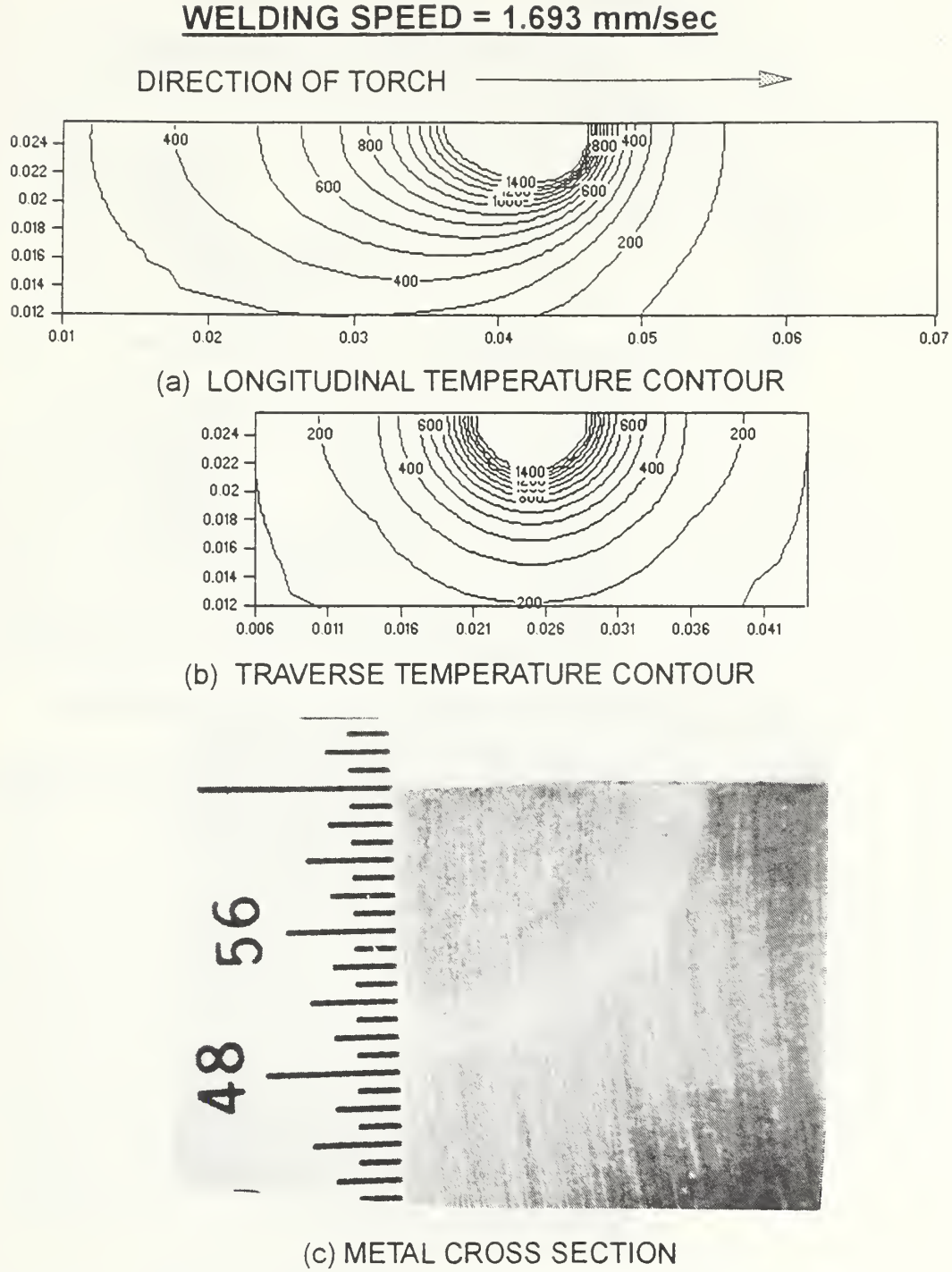

Figure 30. (a) Longitudinal Temperature Contour, (b) Traverse Temperature Contour, and (c) Metal Cross Section for Run #24.

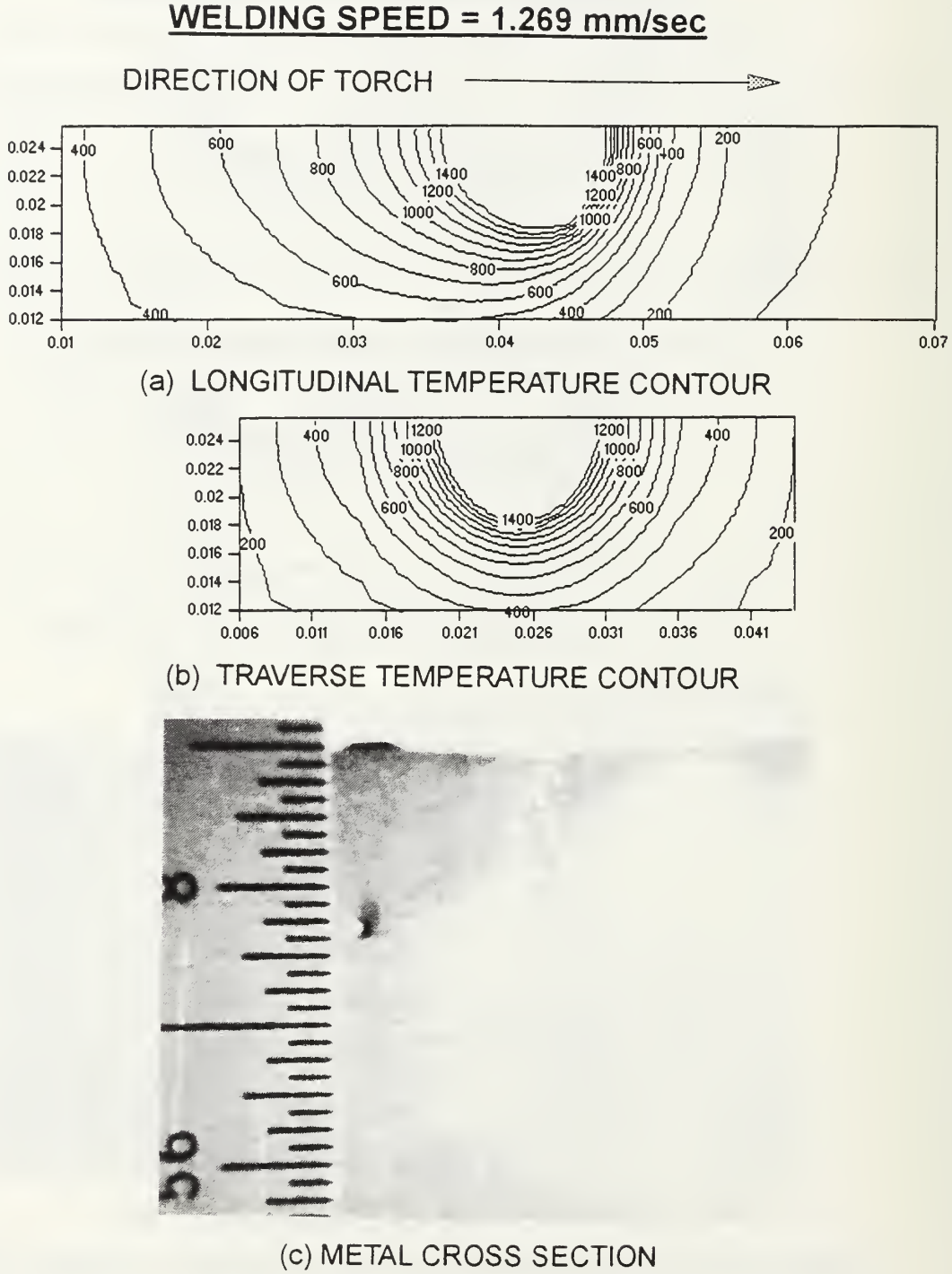

Figure 31. (a) Longitudinal Temperature Contour, (b) Traverse Temperature Contour, and (c) Metal Cross Section for Run #25.

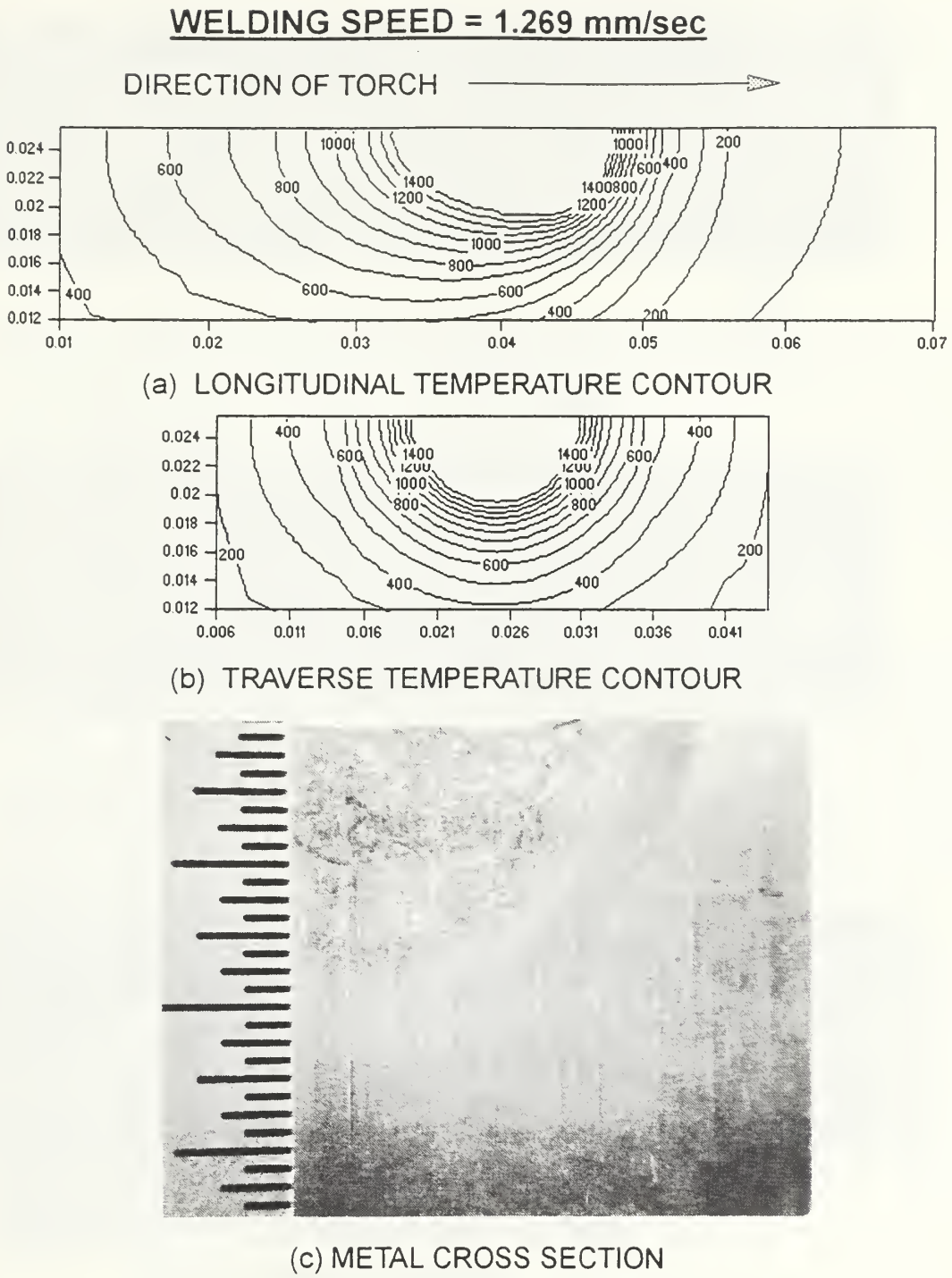

Figure 32. (a) Longitudinal Temperature Contour, (b) Traverse Temperature Contour, and (c) Metal Cross Section for Run #30.

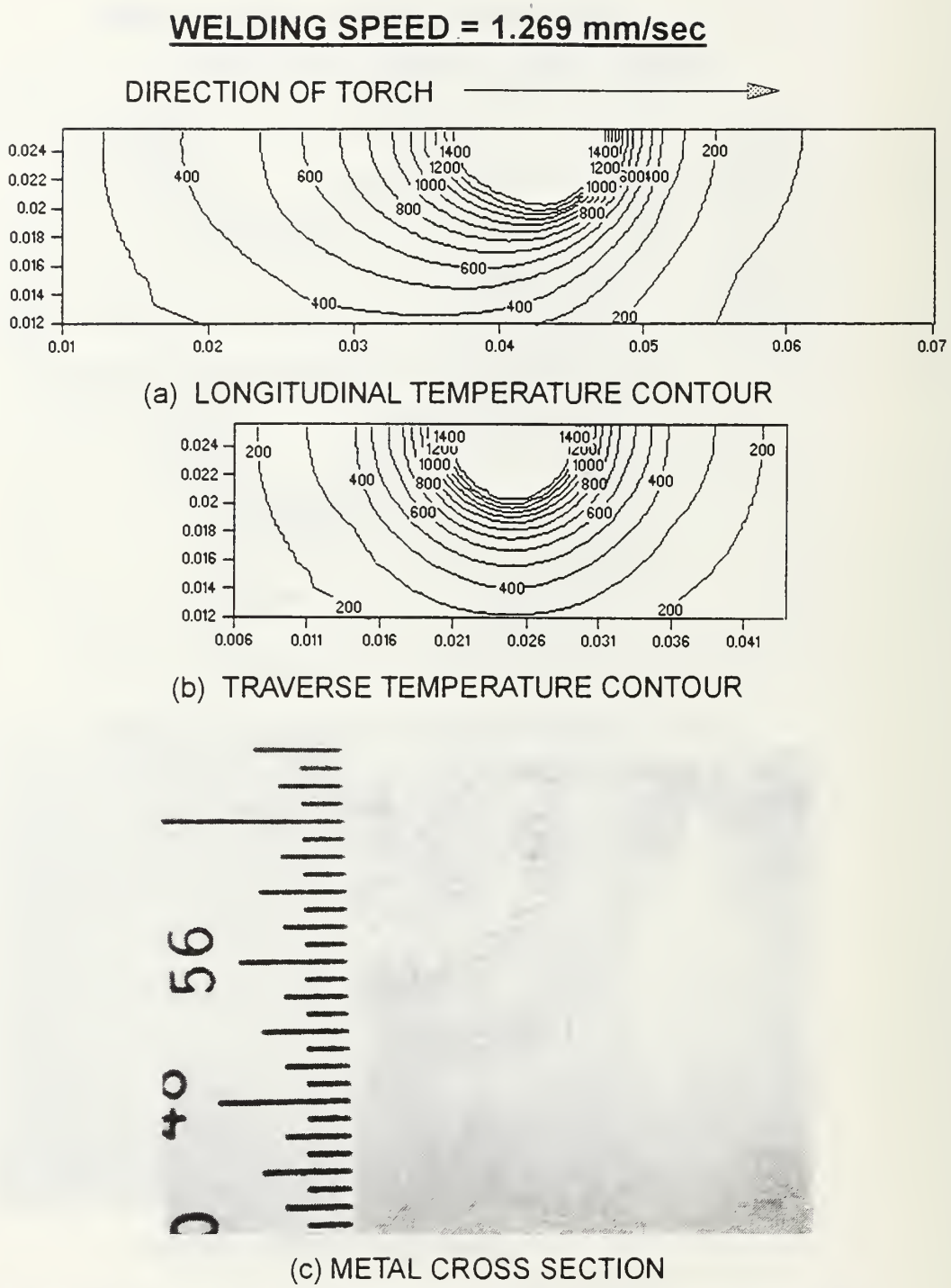

Figure 33. (a) Longitudinal Temperature Contour, (b) Traverse Temperature Contour, and (c) Metal Cross Section for Run #36.

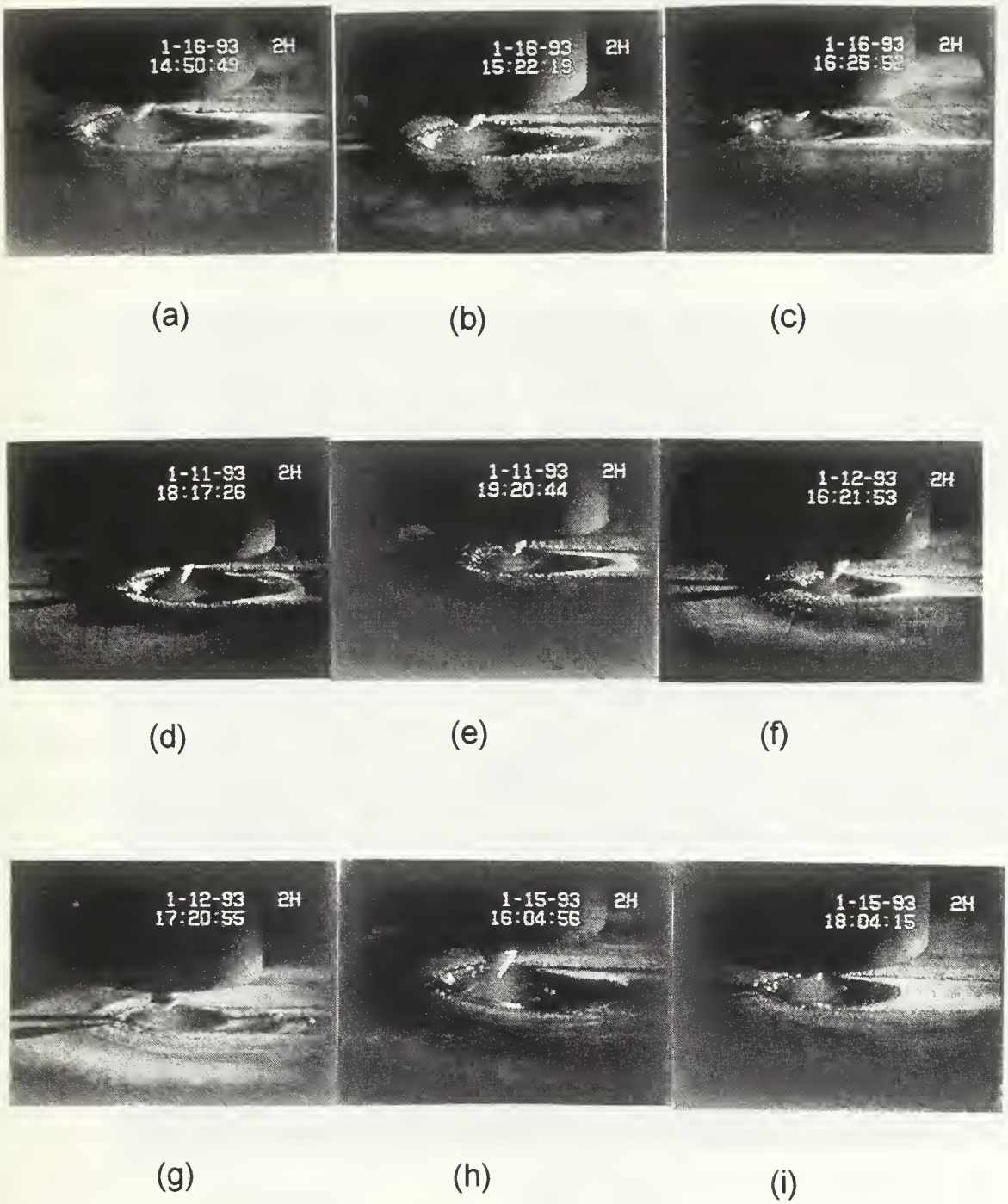

Figure 34. Single Digitized Weld Pool Video Frame Showing the Free Surface.

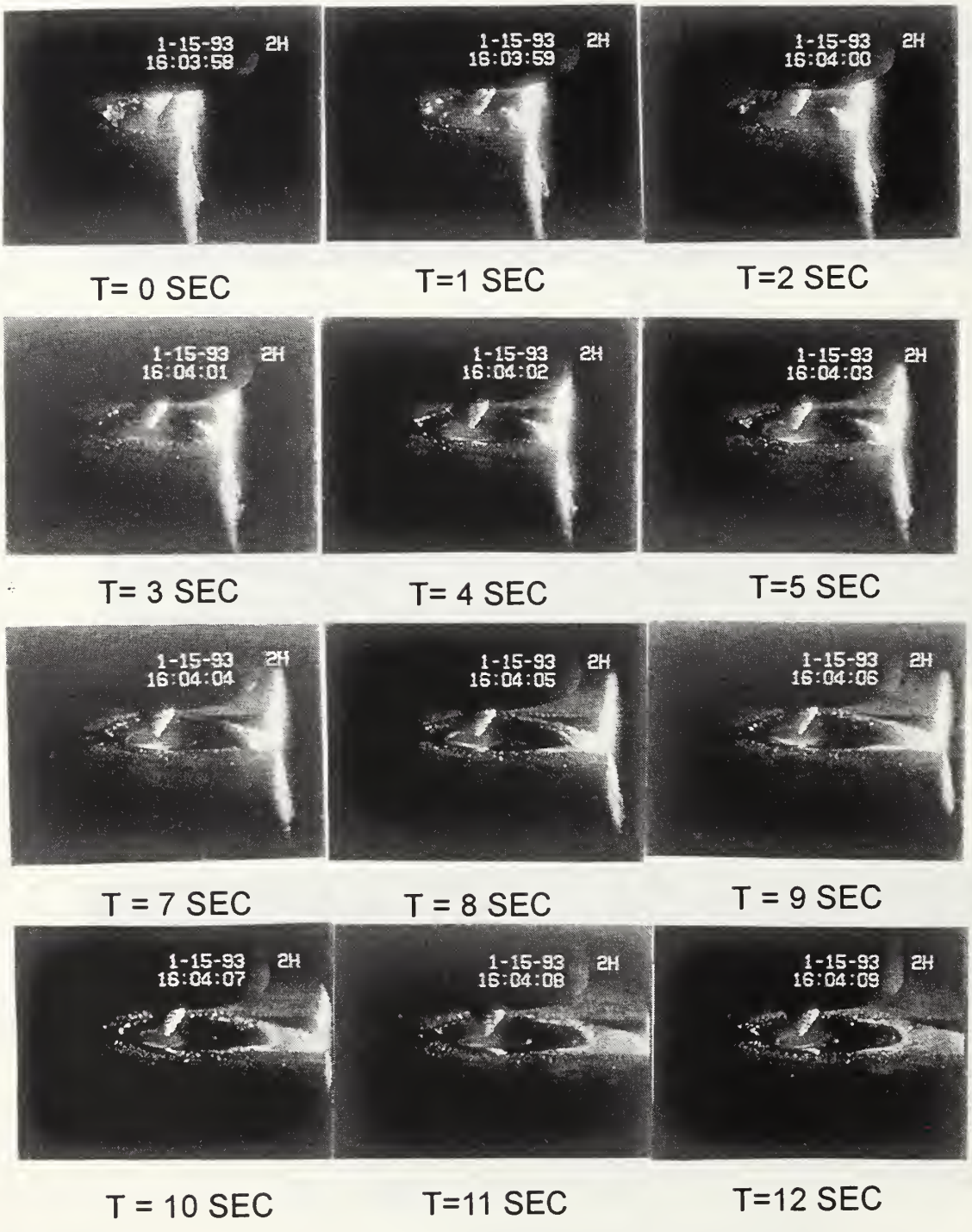

Figure 35. Weld Pool Development Showing the Transient Development within a Period of 12 Seconds at One Second Interval.

V. CONCLUSIONS AND RECOMMENDATIONS

A three dimensional heat conduction model developed based on a double ellipsoid pool shape approximation has been presented for GTAW welding. The present computations revealed a mean value of 72% for the efficiency. The range of present computed values is consistent with calorimetric type measurements in the literature. Since the present technique does not require a calorimetric setup it can be easily implemented in a variety of applications. Even though the results obtained here apply to the GTAW process, the technique is not limited to a particular welding process.

For further research, it is recommended that additional experiments be conducted with different materials and joining processes. The effect of the mesh size in the computations also needs to be investigated further.

LIST OF REFERENCES

1. U.S. Patent 419,032, Jan. 7, 1890, "Methods of Welding by Electricity, " Charles Lewis Coffin, Detroit, Mich.

2. Rosenthal, D., and Schmerber, R., "Thermal Study of Arc Welding - Experimental Verification of Theoretical Formulas," *Welding Journal*, 17, April 1938, pp.2 -8.

3. Rosenthal, D., "Mathematical Theory of Heat Distribution During Welding and Cutting," *Welding Journal*, 20, May 1941, pp. 220s-234s.

4. Rosenthal, D., "The Theory of Moving Sources of Heat and Its Application to Metal Treatments," *Trans. ASME*, 68, Nov 1946, pp. 849-866.

5. Kou, S., *Welding Metallurgy*, John Wiley & Sons, 1987.

6. Christensen, N., Davies, V. de L., and Gjermundsen, K.: *British Welding Journal*, 12: 54, 1965.

7. Ushio, M., Ishimura, T., Matsuda, F., and Arata, Y.: *Trans. Japan Weld. Res. Inst.*,6: 1, 1977.

8. Grosh, R.J., and Trabant, E.A., "Arc Welding Temperatures," *Welding Journal*, 35(8); 1956, pp. 396s-400s.

9. Pavelic, V., Tanbakuchi, R., Uyehara, O.A., and Myers, P.S., "Experimental and Computed Temperature Histories in Gas Tungsten Arc Welding of Thin Plates," *Welding Journal*, 48(7); 1969, pp. 295s-305s.

10. Tsai, C.L., "Parametric Study on Cooling Phenomena in Underwater Welding," PhD Thesis, MIT (1977).

11. Tsai, C.L.,"Modeling of the Thermal Behavior of Metals During Welding," *Trends in Welding Research*, Edited by S.A. David, American Society of Metals, 1981, pp. 91-108.

12. Wilkinson, J.B., and Milner, D.R., Heat Transfer from Arcs, *British Welding Journal*, vol. 7(2), 115-128, 1960.

13. Malmuth, N.D., Hall, W.F., Davis, B.I., and Rosen, C.D., "Transient Thermal Phenomena and Weld Geometry in GTAW," *Welding Journal*, vol.53(9), 388s-400s, 1974.

14. Tsai, N.S., and Eager, T.W., "Distribution of the Heat and Current Fluxes and Gas Tungsten Arcs," *Metallurgical Transactions B*, vol. 16B(4), 841-846, 1985.

15. Giedt, W.H., Tallerico, L.N., and Fuerschbach, P.W., GTA Welding Efficiency: Calometric and Temperature Field Measurements, *Welding Journal*, vol. 68(1), 28-32, 1989.

16. Smartt, H.B., Stewart, J.A., and Einerson, C.J., Heat Transfer in Gas Tungsten Arc Welding, ASM Metals/Materials Series, 8511-011, 1-14, 1986.

17. Goldak, J., Chakravarti, A., and Bibby, M., "A Finite Element Model for Welding Heat Sources," *Metallurgical Transactions*, Volume 15B, June 1984, pp 299-305.

18. Carry,H.B.:Modern Welding Technology, Prentice-Hall, Englewood Cliffs, NJ, 1979.

19. "System Description and Operating Instruction," Model PN-232, Laser Augmented Welding Vision System, *Control Vision Inc.*, Idaho Falls, Idaho.

20. Model UV12 Nitrogen Laser Service Manual, PRA Laser, Inc., November 1987.

21. Mazunder, J., Chen, M.M., Zehr, R., and Voelkel, D., "Effect of Convection on Weld Pool Shape and Macrostructure: Numerical Modeling Portion," Report to U.S. Navy for Research Conducted under Contract No. N00014-89-J-1473, February 1990.

22. Ule, R.L., "A Study of the Thermal Profiles During Autogenous Arc Welding," M.S. and M.E. Thesis, Naval Postgraduate School, Monterey, CA, March 1989.

INITIAL DISTRIBUTION LIST

		No. Copies
1.	Defense Technical Information Center Cameron Station Alexandria VA 22304-6145	2
2.	Library, Code 052 Naval Postgraduate School Monterey CA 93943-5002	2
3.	E.A. Metzbower Naval Research Laboratory Washington, D.C. 20375-5000	1
4.	Department Chairman, Code ME Department of Mechanical Engineering Naval Postgraduate School Monterey, CA 93943-5000	1
5.	Yogendra Joshi, Code ME/Ji Naval Postgraduate School Monterey, CA 93943-5000	2
6.	Richard Morris CODE 2815 David Taylor Research Laboratory Annapolis, MD 21402	1
7.	SEA-05 Naval Sea Systems Command Washington, D.C. 20362-5101	1
8.	SEA-92R Naval Sea Systems Command Washington, D.C. 20362-5101	1
9.	Naval Engineering Curricular Office CODE 34 Naval Postgraduate School Monterey, CA 93943-5000	1

10. Dr. Pradip Dutta, Code ME/Da 1
Naval Postgraduate School
Monterey, CA 93943-5000

11. LCDR(Sel) Candonino P. Franche 3
557 Canyon Dr.
Bonita, CA 91902